

Production of heavy Higgs bosons and decay into top quarks at the LHC

W. Bernreuther ^{a,1}, P. Galler ^{b,2}, C. Mellein ^{a,3}, Z.-G. Si ^{c,4} and P. Uwer ^{b,5}

^aInstitut für Theoretische Teilchenphysik und Kosmologie, RWTH Aachen University,
52056 Aachen, Germany

^bInstitut für Physik, Humboldt-Universität zu Berlin, 12489 Berlin, Germany

^cSchool of Physics, Shandong University, Jinan, Shandong 250100, China

Abstract

We investigate the production of heavy, neutral Higgs boson resonances and their decays to top-quark top-antiquark ($t\bar{t}$) pairs at the Large Hadron Collider (LHC) at next-to-leading order (NLO) in the strong coupling of quantum chromodynamics (QCD). The NLO corrections to heavy Higgs boson production and the Higgs-QCD interference are calculated in the large m_t limit with an effective K-factor rescaling. The nonresonant $t\bar{t}$ background is taken into account at NLO QCD including weak-interaction corrections. In order to consistently determine the total decay widths of the heavy Higgs bosons, we consider for definiteness the type-II two-Higgs-doublet extension of the standard model and choose three parameter scenarios that entail two heavy neutral Higgs bosons with masses above the $t\bar{t}$ threshold and unsuppressed Yukawa couplings to top quarks. For these three scenarios we compute, for the LHC operating at 13 TeV, the $t\bar{t}$ cross section and the distributions of the $t\bar{t}$ invariant mass, of the transverse top-quark momentum and rapidity, and of the cosine of the Collins-Soper angle with and without the two heavy Higgs resonances. For selected $M_{t\bar{t}}$ bins we estimate the significances for detecting a heavy Higgs signal in the $t\bar{t}$ dileptonic and lepton plus jets decay channels.

PACS number(s): 12.38.Bx, 12.60.Fr, 14.65.Ha, 14.80.Ec

Keywords: hadron collider physics, Higgs boson, top quark, QCD corrections, new physics

¹breuther@physik.rwth-aachen.de

²galler@physik.hu-berlin.de

³mellein@physik.rwth-aachen.de

⁴zgsi@sdu.edu.cn

⁵uwer@physik.hu-berlin.de

1. Introduction

The investigations of the production and decays of the 125 GeV spin-zero resonance [1, 2] at the Large Hadron Collider (LHC) by the CMS [3] and ATLAS experiments [4] show that the properties of this particle are consistent with those of the Higgs boson of the standard model (SM). These results strongly support the Higgs mechanism of electroweak symmetry breaking, but do not exclude the possibility that additional Higgs bosons with masses below or around 1 TeV exist. There are several well-known motivations for considering the existence of an extended Higgs sector (for reviews see, for instance, Refs. [5, 6]), and major experimental efforts at the LHC are being devoted to the search for additional spin-zero bosons. To date, these efforts include investigations which were aimed at tracing additional neutral Higgs bosons with significant couplings to the electroweak gauge bosons [7–11] or enhanced couplings (in comparison to respective SM Higgs couplings) to b quarks [12, 13] and charged leptons [14, 15]. These searches—negative so far—have an impact on parts of the parameter spaces of models with an extended Higgs sector but are, needless to say, by far not exhaustive.

One possibility, which is notoriously difficult to explore experimentally, is that one or several neutral Higgs bosons with masses above the top-antitop quark ($t\bar{t}$) production threshold exist, with significant Yukawa couplings to top quarks but suppressed couplings to the weak gauge bosons and to d -type quarks and charged leptons. Very likely, the resonant production of such a Higgs boson ϕ and its subsequent decay into $t\bar{t}$ at the LHC, $pp \rightarrow \phi \rightarrow t\bar{t}X$, does not show up as a resonance bump in the $t\bar{t}$ invariant mass distribution but as a distinctive peak-dip structure. This structure is caused by the interference of the signal and the nonresonant $t\bar{t}$ background amplitudes if the narrow-width approximation does not apply to ϕ , which is very likely the case. This was first shown in Refs. [16, 17] for a scalar and pseudoscalar ϕ , respectively, and in Refs. [18–20] also for a charge parity (CP) mixture. In Refs. [18–20] effects of a heavy Higgs boson on top-quark spin observables were also investigated. More recently, the study of this ϕ decay channel was taken up again in Refs. [21–26]. All these investigations were performed at leading-order (LO) QCD.

First experimental attempts to search for heavy spin-zero states ϕ in the $t\bar{t}$ decay channel at the LHC were made by the CMS [27] and ATLAS [28] experiments. These investigations are difficult, in particular because the experimental resolution of the $t\bar{t}$ invariant mass is, in general, larger than the expected width of ϕ , which hampers a resolution of the resonance region. On the theoretical side, a more precise description of the reaction $pp \rightarrow \phi \rightarrow t\bar{t}X$ is necessary. In this paper we investigate the resonant production of heavy neutral Higgs bosons ϕ and their decay into $t\bar{t}$ including an approximate calculation of the next-to-leading order QCD corrections. That is, the NLO Higgs production amplitudes are computed in the limit of $m_t \rightarrow \infty$. The interferences of the signal and nonresonant $t\bar{t}$ background amplitudes are also determined at NLO QCD. The nonresonant $t\bar{t}$ background is computed at NLO QCD and the mixed QCD-weak interaction corrections are included. We analyze how heavy Higgs bosons affect the $t\bar{t}$ cross section and several distributions. In particular, we determine the shape of the $t\bar{t}$ invariant mass distribution in the vicinity of a heavy Higgs resonance, which is of primary interest. We have analyzed the reaction at hand for arbitrary configurations of the t and \bar{t} spins,

but we defer the investigation of heavy Higgs boson effects on $t\bar{t}$ spin correlations and on the t and \bar{t} polarization to a future publication.

The NLO QCD analysis of $pp \rightarrow \phi \rightarrow t\bar{t}X$ presented here may be applied to a number of SM extensions. Yet, in applications one has to fix the number of heavy Higgs bosons which can be resonantly produced in the $t\bar{t}$ channel. Other important ingredients in this analysis are the total widths of the Higgs bosons ϕ with mass larger than twice the top-quark mass. These widths must be computed in a concrete model, in order to maintain the unitarity of the S matrix. For definiteness we have chosen to analyze the process at hand within the type-II two-Higgs-doublet extension (2HDM) of the standard model. This model, which may be realized with or without Higgs sector CP violation, is among the simplest extensions of the SM. While interesting per se, it may also be considered a prototype of an extended Higgs/spin-zero sector. (For a recent review see, e.g., Ref. [6].) The spectrum of physical spin-zero particles of 2HDMs consists of three neutral Higgs bosons ϕ_1, ϕ_2, ϕ_3 and a charged Higgs boson and its antiparticle, H^\pm . We identify ϕ_1 with the observed 125 GeV resonance and assume that the masses ϕ_2 and ϕ_3 are larger than twice the top-quark mass. The charged Higgs boson is assumed to be heavy enough as to play no role in our analysis. The LHC results on the 125 GeV Higgs resonance imply that the parameters of 2HDMs are constrained by the requirement of ϕ_1 being SM-like. In addition we are interested in parameter scenarios where the top-quark Yukawa couplings of the heavy Higgs bosons ϕ_2, ϕ_3 are somewhat enhanced or at least as large as the SM top-quark Yukawa coupling—without simultaneous enhancement of the Yukawa couplings of d -type quarks and charged leptons—and where the couplings of ϕ_2, ϕ_3 to the weak gauge bosons are severely suppressed. This is possible in the type-II 2HDM. We define three such parameter scenarios which are in accord with experimental constraints—two scenarios with CP conservation and one with CP violation in the tree-level Higgs potential. For each of these parameter scenarios, we compute the Higgs boson contributions to the $t\bar{t}$ cross section and to several top-quark distributions, in particular the $t\bar{t}$ invariant mass distribution, for the LHC at 13 TeV. In the context of our type-II 2HDM parameter scenarios the NLO analysis is organized as follows: the nonresonant contribution of ϕ_1 is part of the mixed QCD-weak interaction corrections to the nonresonant $t\bar{t}$ background. As to the amplitudes of $ab \rightarrow \phi_j \rightarrow t\bar{t}X$ ($j = 2, 3$), where a, b denote partons, their interference with the nonresonant $t\bar{t}$ amplitudes is taken into account. In the case of neutral Higgs-sector CP violation, the ϕ_2 and ϕ_3 production amplitudes interfere also among each other but, as shown below, this contribution is very small for our parameter scenarios and can be neglected. The evaluation of our three parameter scenarios exemplifies the significance of the QCD corrections, but the effect of the two heavy Higgs bosons on the top-quark distributions is, overall, rather small. Nevertheless, statistically significant signals are possible. We propose to analyze existing and future LHC $t\bar{t}$ data by scanning the distribution of the $t\bar{t}$ invariant mass, $M_{t\bar{t}}$, with a sliding $M_{t\bar{t}}$ window of width ~ 80 GeV.

The paper is organized as follows. In Sec. 2 we briefly recapitulate the main features of the type-II 2HDM with and without Higgs-sector CP violation that are relevant for our analysis. In Sec. 3 we define three parameter scenarios which we use in the following: two sets associated with a CP -conserving and one set related to a CP -violating Higgs potential. We discuss that

our scenarios are compatible with existing experimental constraints on the parameter space of the type-II 2HDM. Section 4 contains the setup of our calculations. For illustrative purposes we discuss first the resonant production of heavy Higgs bosons and their decay to $t\bar{t}$ and the interference with the nonresonant background at LO QCD. Then we outline how we compute distributions for this reaction including the Higgs-QCD interference at NLO QCD and we describe our K-factor approximation adapted from Ref. [29]. The nonresonant $t\bar{t}$ background is incorporated at NLO QCD including the weak-interaction corrections. Section 5 contains the results for $t\bar{t}$ production at the LHC (13 TeV) for the three parameter scenarios introduced in Sec. 3. First we compute the inclusive $t\bar{t}$ cross section and the $M_{t\bar{t}}$ distribution without and with the two heavy Higgs resonances. We estimate, for appropriately chosen $M_{t\bar{t}}$ intervals and for our three parameter scenarios, the significance with which a heavy Higgs signal could be detected in the $t\bar{t}$ dileptonic and lepton plus jets decay channels. Furthermore, we give the distributions of the rapidity and transverse momentum of the top quark and the distributions of the cosine of the Collins-Soper angle [30] for selected $M_{t\bar{t}}$ windows. Moreover we show that the negative experimental searches for heavy spin-zero resonances in the $t\bar{t}$ channel [27, 28] at the LHC (8 TeV) do not exclude our parameter scenarios. We conclude in Sec. 6. Appendix A contains a discussion of the complex mass scheme that we apply for the description of the heavy Higgs boson resonances. The cancellation of real and virtual nonfactorizable QCD corrections to $gg \rightarrow \phi_j \rightarrow t\bar{t}$ in the soft gluon approximation (SGA) is outlined in Appendix B.

2. The type-II two-Higgs-doublet model

As mentioned above, we choose the type-II two-Higgs-doublet model as an example of a SM extension which allows one to describe, in a consistent field-theoretic and phenomenologically viable way, both the 125 GeV Higgs resonance and additional neutral heavy Higgs bosons. In this section we shortly describe the salient features of several variants of this model which are relevant for our analysis.

In 2HDMs the SM field content is extended by an additional Higgs doublet. Both Higgs doublets Φ_1 and Φ_2 transform under $SU(3)_c \times SU(2)_L \times U(1)_Y$ as $(1, 2, 1/2)$.

The type-II model is defined by its Yukawa coupling structure: the doublet Φ_1 is coupled to right-chiral down-type quarks and charged leptons, while Φ_2 is coupled to right-chiral up-type quarks only. The type-II model belongs to those 2HDMs where, by construction, flavor-changing neutral currents are absent at tree level. The most general Hermitian, gauge invariant and renormalizable 2HDM potential reads (see, for instance, [6]):

$$\begin{aligned}
V(\Phi_1, \Phi_2) = & -\mu_1^2 |\Phi_1|^2 - \mu_2^2 |\Phi_2|^2 - (\mu_3^2 \Phi_1^\dagger \Phi_2 + \text{h.c.}) \\
& + \frac{\lambda_1}{2} |\Phi_1|^4 + \frac{\lambda_2}{2} |\Phi_2|^4 + \lambda_3 |\Phi_1|^2 |\Phi_2|^2 + \lambda_4 |\Phi_1^\dagger \Phi_2|^2 \\
& + \left[\frac{\lambda_5}{2} (\Phi_1^\dagger \Phi_2)^2 + \lambda_6 (\Phi_1^\dagger \Phi_1) (\Phi_1^\dagger \Phi_2) + \lambda_7 (\Phi_2^\dagger \Phi_2) (\Phi_1^\dagger \Phi_2) + \text{h.c.} \right], \quad (1)
\end{aligned}$$

with real $\mu_1^2, \mu_2^2, \lambda_{1,2,3,4}$ and complex $\mu_3^2, \lambda_{5,6,7}$, adding up to 14 independent real parameters.

Three of the 14 parameters can be eliminated by a change of basis, $\Phi'_i = U_{ij}\Phi_j$, where U is a unitary 2×2 matrix.

After electroweak gauge symmetry breaking, using the unitary gauge the two-Higgs doublets take the form

$$\begin{aligned}\Phi_1 &= \left(-H^+ \sin\beta, \frac{1}{\sqrt{2}}(v_1 + \varphi_1 - iA \sin\beta) \right)^T, \\ \Phi_2 &= e^{i\xi} \left(H^+ \cos\beta, \frac{1}{\sqrt{2}}(v_2 + \varphi_2 + iA \cos\beta) \right)^T,\end{aligned}\quad (2)$$

where $\tan\beta = v_2/v_1$ is the ratio of the vacuum expectation values of the two-Higgs-doublet fields with $v = \sqrt{v_1^2 + v_2^2} = 246$ GeV. By a field redefinition the phase ξ can be put to zero without loss of generality. The field H^+ describes the physical charged Higgs boson of the model, while $\varphi_{1,2}$ and A are the physical neutral CP -even and CP -odd field degrees of freedom. The Higgs potential (1) leads to mixing among these neutral fields. We denote the neutral Higgs fields and the associated Higgs particles of definite mass by ϕ_j , $j = 1, 2, 3$. They are related to $\varphi_{1,2}$ and A by an orthogonal transformation, $(\phi_1, \phi_2, \phi_3)^T = R(\varphi_1, \varphi_2, A)^T$. We parametrize the orthogonal matrix R as follows:

$$R = \begin{pmatrix} c_1 c_2 & c_2 s_1 & s_2 \\ -c_1 s_2 s_3 - c_3 s_1 & c_1 c_3 - s_1 s_2 s_3 & c_2 s_3 \\ -c_1 c_3 s_2 + s_1 s_3 & -c_1 s_3 - c_3 s_1 s_2 & c_2 c_3 \end{pmatrix}, \quad (3)$$

where c_i and s_i ($i = 1, 2, 3$) are the cosines and sines of the mixing angles α_i . Due to the symmetries of R [31] one can restrict the range of the angles to $-\pi/2 \leq \alpha_i < \pi/2$.

The Higgs potential in its general form (1) violates the CP symmetry and, as a consequence, the CP -even and CP -odd Higgs fields mix and the mass eigenstates ϕ_j ($j = 1, 2, 3$) do not have a definite CP . In this general CP -violating version of the type-II 2HDM, the Higgs potential has, as mentioned above, 11 independent parameters.¹ For phenomenological studies it is useful to choose as independent parameters a different set, in terms of which the parameters of the potential can be expressed. This set includes the following nine parameters which we call phenomenological parameters:

$$m_1, m_2, m_3, m_+, \alpha_1, \alpha_2, \alpha_3, \tan\beta, v, \quad (4)$$

where m_j ($j = 1, 2, 3$) are the masses of the three neutral Higgs bosons and m_+ is the mass of H^+ . The value of v is of course fixed by experiment.

In order to motivate the type-II 2HDM construction by a symmetry argument, one often imposes a Z_2 symmetry onto the model which may be softly broken by the Higgs potential. This approximate symmetry implies that the hard Z_2 symmetry-breaking terms in (1) are absent, $\lambda_6 = \lambda_7 = 0$. This variant of the model still allows for neutral Higgs sector CP violation [33], i.e., for the mixing of $\varphi_{1,2}$ and A , if $\text{Im}(\lambda_5/\mu_3^4) \neq 0$. One can show [34] that in this case the

¹For a general discussion, see Ref. [32].

number of independent phenomenological parameters listed in (4) is reduced by one. In the model with approximate Z_2 symmetry where $\text{Im}\lambda_5 \neq 0$, one can, for instance, express the mass m_3 of the neutral Higgs boson ϕ_3 in terms of $m_1, m_2, \tan\beta$, and the Higgs mixing angles α_i ($i = 1, 2, 3$). In our applications below, where we consider also the case of Higgs sector CP violation, we however refer to the more general case where (4) is an independent parameter set, in order to avoid a theoretical bias.

The type-II 2HDM where the Higgs potential conserves CP is a special case and is also of great phenomenological interest. In this case only φ_1 and φ_2 mix. This is described by the mixing angle α_1 , while $\alpha_2 = \alpha_3 = 0$. The matrix R is now block diagonal with $R_{13} = R_{23} = R_{31} = R_{32} = 0$ and $R_{33} = 1$. The two CP -even and the CP -odd neutral mass eigenstates are often conventionally denoted by $\phi_1 = h$, $\phi_2 = H$, and $\phi_3 = A$. The type-II 2HDM with CP -conserving Higgs potential may be motivated by assuming an approximate Z_2 symmetry. Then the potential has eight independent parameters, but they are reduced by one by the condition that the ground state of the model does not break CP spontaneously. Thus, one may choose as independent parameters the following set:

$$m_1, m_2, m_3, m_+, \alpha_1, \tan\beta, v. \quad (5)$$

In the following we identify the 125 GeV Higgs resonance with the Higgs boson ϕ_1 and assume that the masses of the two other neutral states $\phi_{2,3}$ lie above the $t\bar{t}$ threshold. In addition, we assume that the mass of the charged Higgs boson H^\pm is of the order of the masses of $\phi_{2,3}$, so that the two-body decays $\phi_{2,3} \rightarrow W^\pm H^\mp$ are kinematically excluded. Fits to LHC data [3, 4] imply that the couplings of the 125 GeV Higgs boson to the third-generation fermions and gauge bosons are not too different from those of the SM Higgs boson. In the context of the CP -conserving 2HDM this means that the model is close to the so-called alignment limit² $\beta = \alpha_1$. Yet, at present the uncertainties on the measured couplings of the 125 GeV resonance are still rather large, $\sim 20\% - 30\%$. In particular it is not yet experimentally shown that the 125 GeV resonance is a pure CP -even state—a pseudoscalar admixture is still a possibility. Nevertheless, in the scenarios which we define in the next section and apply subsequently we shall choose parameters in or close to the alignment limit.

For our analysis below we need the interactions of the neutral Higgs bosons with fermions and weak gauge bosons, and their interactions among each other. We parametrize the couplings of the ϕ_j to the quarks and charged leptons $f = q, \ell$ and to weak gauge boson pairs in the type-II model with Higgs sector CP violation as follows:

$$\mathcal{L}_1 = -\frac{m_f}{v} (a_{jf} \bar{f}f - b_{jf} \bar{f}i\gamma_5 f) \phi_j + f_{jVV} \phi_j \left(\frac{2m_W^2}{v} W_\mu^- W^{+\mu} + \frac{m_Z^2}{v} Z_\mu Z^\mu \right), \quad (6)$$

where a sum over f and $j = 1, 2, 3$ is implicit. The reduced scalar and pseudoscalar Yukawa couplings a_{jf} and b_{jf} and the reduced couplings f_{jVV} depend on the values of $\tan\beta$ and on

²Often the parametrization of the mixing matrix R used in the literature is different from (3). For instance, in the parametrizations of [34, 35], $\alpha = \alpha_1 - \pi/2$; i.e., the alignment limit is then given by $\beta - \alpha = \pi/2$.

the elements R_{ij} of the Higgs mixing matrix (3) and are listed in Table 1. The couplings f_{jVV} satisfy the sum rule

$$\sum_{j=1}^3 f_{jVV}^2 = 1. \quad (7)$$

The interaction of neutral Higgs bosons ϕ_j, ϕ_l ($j \neq l$) with the Z boson is given by

$$\mathcal{L}_2 = -\frac{g_W}{2\cos\theta_W} f_{Zjl} Z^\mu \phi_j \overleftrightarrow{\partial}_\mu \phi_l, \quad (8)$$

where g_W is the $SU(2)_L$ gauge coupling and θ_W denotes the weak mixing angle. For computing the rates of the decays $\phi_j \rightarrow Z\phi_1$ ($j = 2, 3$), we need the couplings f_{Zj1} . They are given by

$$f_{Zj1} = (-\sin\beta R_{11} + \cos\beta R_{12})R_{j3} - (-\sin\beta R_{j1} + \cos\beta R_{j2})R_{13}. \quad (9)$$

Moreover, for computing the decays $\phi_j \rightarrow 2\phi_1$ ($j = 2, 3$) the trilinear neutral Higgs couplings are required, $\mathcal{L}_3 = g_{ijl}\phi_i\phi_j\phi_l$. In the CP -violating type-II 2HDM the couplings g_{ijl} have a quite complicated form. They were derived in terms of the potential parameters in [35] and in terms of the phenomenological parameters in [36].

Table 1: Reduced couplings to quarks, leptons and gauge bosons of the neutral Higgs bosons ϕ_j of the type-II 2HDM in the parametrization (6). The labels t, b , and τ are placeholders for u -type, d -type quarks, and charged leptons.

a_{jt}	$a_{jb} = a_{j\tau}$	b_{jt}	$b_{jb} = b_{j\tau}$	f_{jVV}
$R_{j2}/\sin\beta$	$R_{j1}/\cos\beta$	$R_{j3}\cot\beta$	$R_{j3}\tan\beta$	$\cos\beta R_{j1} + \sin\beta R_{j2}$

3. Three type-II 2HDM scenarios

In this section we define three phenomenologically viable parameter sets for the type-II 2HDM, two for the CP -conserving and one for the CP -violating variant, which we use in the next sections. We compute for these parameter sets the total widths of the heavy neutral Higgs bosons ϕ_2, ϕ_3 , including QCD corrections. As already mentioned above, in all three cases we identify the 125 GeV Higgs boson with ϕ_1 and choose the parameters such that its couplings to fermions and gauge bosons are SM-like. For the parameter sets below, the total width Γ_1 of ϕ_1 is of the order of 4 MeV. This width plays no role in the computations of Secs. 4–5. For the masses of the two other neutral Higgs bosons we assume $m_2, m_3 > 2m_t$. The resonant production of ϕ_2, ϕ_3 has a chance of being experimentally detectable in the $t\bar{t}$ decay channel only if the Yukawa couplings are not suppressed in comparison with the SM top-Yukawa coupling. Therefore we choose $\tan\beta = 0.7$ for all three scenarios below. Experimental constraints from

B physics require that for $\tan\beta < 1$ the mass m_+ of the charged Higgs boson is large. In order to satisfy these constraints [37–39] we assume that $m_+ > 720$ GeV. This implies for the parameter scenarios below that the decays $\phi_{2,3} \rightarrow W^\pm H^\mp$ cannot occur.

We determine the total widths of ϕ_2 and ϕ_3 by computing the sum of the largest two-body decay rates. The QCD corrections to the decays $\phi_j \rightarrow q\bar{q}$ and $\phi_j \rightarrow gg$ may be computed with the computer program HDECAY [40] or 2HDMC [41]. Both codes apply only to CP -conserving 2HDM but can be easily adapted to CP -violating scenarios. Since both programs use the renormalization scale $\mu = m_\phi$, which is not suited for our applications (see below), we use the expressions for the partial decay rates to quarks and to gluons including QCD corrections from Refs. [42, 43] and Ref. [44], respectively. Expressions for the other decay rates (including the CP -violating case) can also be found in the literature, see e.g. Ref. [35]. Where possible we checked our results with 2HDMC. In these computations we use the top-quark mass m_t in the on-shell scheme and put $m_t = 173.34$ GeV. Moreover, in order to be consistent with our computations of Secs. 4–5 we consider the following values and variations of the renormalization scale μ :

$$\frac{\mu_0}{2} \leq \mu \leq 2\mu_0, \quad \mu_0 = \frac{m_2 + m_3}{4}. \quad (10)$$

Electroweak corrections to the decays $\phi_j \rightarrow f\bar{f}$ [45] and $\phi_j \rightarrow VV$ [46] are sizeable, especially for heavy Higgs bosons. Because we consider parameter scenarios where the $\phi_j VV$ couplings are suppressed for $j = 2, 3$, these corrections to $\phi_j \rightarrow VV$ will not affect the total widths $\Gamma_{2,3}$ very much. The electroweak corrections to $\phi_j \rightarrow t\bar{t}$ can be as large as the QCD corrections. Because we analyze in Sec. 4 resonant hadronic heavy Higgs boson production and decay to $t\bar{t}$ only to lowest order in the non-QCD couplings, we omit the contributions of the electroweak corrections to $\Gamma_{2,3}$.

3.1. Scenario 1

We consider the type-II model with a CP -conserving Higgs potential. We choose

$$\tan\beta = 0.7, \quad \alpha_1 = \beta = 0.611, \quad \alpha_2 = \alpha_3 = 0, \quad (11)$$

and choose the following Higgs boson masses, with ϕ_2 and ϕ_3 being nearly mass degenerate:

$$m_1 = 125 \text{ GeV}, \quad m_2 = 550 \text{ GeV}, \quad m_3 = 510 \text{ GeV}, \quad m_+ > 720 \text{ GeV}. \quad (12)$$

That is, ϕ_1 and ϕ_2 are chosen to be pure scalars while ϕ_3 is a pseudoscalar Higgs boson, cf. Table 2. The reduced Yukawa couplings and couplings to the weak gauge bosons, which result from (11) and the formulas of Table 1, are given in Table 2. Recall that a pseudoscalar Higgs boson has no tree-level couplings to W^+W^- and ZZ ($f_{3VV} = 0$). The choice $\alpha_1 = \beta$ puts the model into the alignment limit. Therefore we have also $f_{2VV} = 0$.

We compute the largest two-body decay rates of the scalar ϕ_2 and the pseudoscalar ϕ_3 and determine their total widths by adding up these rates. The leading-order decay-rate formulas

Table 2: Values of the reduced couplings to the third-generation fermions and gauge bosons of the neutral Higgs bosons ϕ_j for the parameter set (11) which is used in scenarios 1 and 2.

	a_{jt}	$a_{jb} = a_{j\tau}$	b_{jt}	$b_{jb} = b_{j\tau}$	f_{jVV}
ϕ_1	1	1	0	0	1
ϕ_2	1.429	-0.700	0	0	0
ϕ_3	0	0	1.429	0.700	0

Table 3: Dominant partial decay widths and the total widths of the two heavy, neutral Higgs bosons ϕ_2 and ϕ_3 in our CP -conserving 2HDM scenario 1, defined in (11)–(12). The super- and subscripts denote the shift due to the scale variations (10).

	Γ_2 [GeV]	Γ_3 [GeV]
$\phi_i \rightarrow t\bar{t}$	$34.48^{+0.33}_{-0.28}$	$49.15^{+0.38}_{-0.32}$
$\phi_i \rightarrow gg$	$0.08^{+0.01}_{-0.01}$	$0.13^{+0.02}_{-0.02}$
Total	$34.56^{+0.34}_{-0.28}$	$49.28^{+0.40}_{-0.34}$

for $\phi_j \rightarrow f\bar{f}, VV, Z\phi_l, 2\phi_l, gg$, where $V = W, Z$, are well-known and are not reproduced here (see, e.g., [41]). The relevant tree-level couplings are given in Sec. 2. The trilinear neutral Higgs couplings are taken from [35, 36] and we use the QCD corrections to $\phi_{2,3} \rightarrow t\bar{t}, gg$ given in Ref. [42–44]. The results are listed in Table 3. The uncertainties result from varying the renormalization scale according to (10). The partial decay widths of $\phi_j \rightarrow f\bar{f}$ ($f \neq t$), $\phi_j \rightarrow \gamma\gamma$, and $\phi_j \rightarrow Z\gamma$ are a few 10^{-3} GeV or smaller and are neglected in the total widths Γ_2, Γ_3 . In particular, the decay rate to $b\bar{b}$ is small because the Yukawa couplings to down-type quarks are not enhanced (Table 2) due to our choice of $\tan\beta < 1$. Moreover, to lowest order in the non-QCD couplings the partial decay rates for $\phi_i \rightarrow VV$, $\phi_i \rightarrow \phi_1 Z$, and $\phi_i \rightarrow \phi_1 \phi_1$ are zero.

3.2. Scenario 2

We choose again a CP -conserving neutral Higgs sector scenario with the same set of angles, Eq. (11), as in scenario 1. Here we assume that the pseudoscalar ϕ_3 is significantly heavier than the scalar ϕ_2 . We choose

$$m_1 = 125 \text{ GeV}, \quad m_2 = 550 \text{ GeV}, \quad m_3 = 700 \text{ GeV}, \quad m_+ > 720 \text{ GeV}. \quad (13)$$

The values of the reduced couplings of ϕ_2, ϕ_3 to the third-generation fermions and gauge bosons given in Table 2 apply also here. The results for the most important two-body decay widths and the total widths of ϕ_2, ϕ_3 are given in Table 4. To lowest order in the non-QCD couplings the partial decay rates for $\phi_i \rightarrow VV$, $\phi_i \rightarrow \phi_1 Z$, $\phi_i \rightarrow \phi_1 \phi_1$, and $\phi_3 \rightarrow \phi_1 \phi_2$ are zero.

Notice that the decay widths for $\phi_2 \rightarrow VV$, $\phi_2 \rightarrow \phi_1\phi_1$ and $\phi_3 \rightarrow Z\phi_1$ vanish in scenarios 1 and 2, respectively, because we have chosen the exact alignment limit $\alpha_1 = \beta$. The more one moves away from this limit, the larger the contributions of these modes will be to the total decay widths.

Table 4: Dominant partial decay widths and total widths of the two heavy, neutral Higgs bosons ϕ_2 and ϕ_3 in our CP -conserving 2HDM scenario 2, defined in (11) and (13). The super- and subscripts denote the shift due to the scale variations (10).

	Γ_2 [GeV]	Γ_3 [GeV]
$\phi_i \rightarrow t\bar{t}$	$34.41^{+0.32}_{-0.26}$	$71.97^{-0.15}_{+0.13}$
$\phi_i \rightarrow \phi_2 Z$	0	3.14
$\phi_i \rightarrow gg$	$0.08^{+0.01}_{-0.01}$	$0.17^{+0.01}_{-0.01}$
Total	$34.49^{+0.33}_{-0.27}$	$75.28^{-0.14}_{+0.11}$

3.3. Scenario 3

We consider a type-II model with a CP -violating Higgs potential (without approximate Z_2 symmetry) such that (4) forms a set of independent parameters. For $\tan\beta$ and the Higgs mixing angles we choose

$$\tan\beta = 0.7, \quad \alpha_1 = \beta, \quad \alpha_2 = \frac{\pi}{15}, \quad \alpha_3 = \frac{\pi}{4}. \quad (14)$$

We set the Higgs boson masses to the values

$$m_1 = 125 \text{ GeV}, \quad m_2 = 500 \text{ GeV}, \quad m_3 = 800 \text{ GeV}, \quad m_+ > 720 \text{ GeV}. \quad (15)$$

Using Table 1 and the parameters (14) we get the values of the reduced Yukawa couplings and couplings to the weak gauge bosons listed in Table 5. As this table shows, in this scenario the three neutral Higgs bosons $\phi_{1,2,3}$ are CP mixtures.

Table 5: Values of the reduced couplings to the third-generation fermions and gauge bosons of the neutral Higgs bosons ϕ_j for the parameter set (14) of scenario 3.

	a_{jt}	$a_{jb} = a_{j\tau}$	b_{jt}	$b_{jb} = b_{j\tau}$	f_{jVV}
ϕ_1	0.978	0.978	0.297	0.146	0.978
ϕ_2	0.863	-0.642	0.988	0.484	-0.147
ϕ_3	-1.157	0.348	0.988	0.484	-0.147

The results for the most important two-body decay widths and the total widths of ϕ_2, ϕ_3 are given in Table 6. In this scenario without approximate Z_2 symmetry we have to specify also

Table 6: Dominant partial decay widths and total widths of the two heavy, neutral Higgs bosons ϕ_2 and ϕ_3 in our CP -violating 2HDM scenario 3, defined in (14)–(15). The super- and subscripts denote the shift due to the scale variations (10).

	Γ_2 [GeV]	Γ_3 [GeV]
$\phi_i \rightarrow t\bar{t}$	$32.31^{+0.31}_{-0.26}$	$85.05^{-0.30}_{+0.25}$
$\phi_i \rightarrow VV$	1.12	5.11
$\phi_i \rightarrow \phi_1 Z$	0.65	3.24
$\phi_i \rightarrow \phi_2 Z$	0	31.28
$\phi_i \rightarrow \phi_1 \phi_1$	2.38	3.00
$\phi_i \rightarrow \phi_1 \phi_2$	0	0.31
$\phi_i \rightarrow gg$	$0.08^{+0.01}_{-0.01}$	$0.17^{+0.01}_{-0.01}$
Total	$36.55^{+0.32}_{-0.27}$	$128.16^{-0.29}_{+0.24}$

the values of the complex parameters λ_6, λ_7 in the 2HDM potential. These parameters only enter the calculation of the decay widths which involve trilinear Higgs couplings, i.e. only the decays $\phi_i \rightarrow \phi_1 \phi_1$ and $\phi_i \rightarrow \phi_1 \phi_2$ listed in Table 6. We choose $\text{Re}\lambda_6 = 0$, $\text{Im}\lambda_6 = -3.677$ and $\lambda_7 = 0$.

3.4. Experimental constraints

The Higgs couplings and masses chosen in the three scenarios above are compatible with existing experimental constraints. As to the couplings of ϕ_1 , in scenarios 1 and 2 the couplings of ϕ_1 are identical to those of the SM Higgs boson. In the CP -violating scenario ϕ_1 has a pseudoscalar component. Nevertheless, also in this scenario the couplings of ϕ_1 given in Table 5 lie within the respective coupling ranges of the 125 GeV boson determined by the CMS [3] and ATLAS [4] experiments, which allow $\sim 20\% - 30\%$ deviations from the respective SM Higgs couplings. Because in our scenarios the tree-level couplings of ϕ_2, ϕ_3 to b quarks, τ leptons, weak gauge bosons, and to ϕ_1 are very small or even zero, the negative searches, so far, at the LHC for nonstandard heavy resonances decaying to W^+W^- [11], ZZ [7, 11], $Z\phi_1$ [8, 10], $\phi_1\phi_1$ [9, 13], $\tau^-\tau^+$ [14, 15], $b\bar{b}$ [12] do not exclude the above scenarios. We comment in Sec. 5 on the CMS [27] and ATLAS [28] searches in the $t\bar{t}$ decay channel.

The nonobservation of deviations from the SM predictions in B-physics data places limits on $\tan\beta$ and on the mass m_+ of the charged Higgs boson. These parameters control the contribution of H^\pm to loop-induced observables like the rare decays $B \rightarrow X_s + \gamma$ and neutral $B_d^0 - \bar{B}_d^0$ mixing. In general the loop effects of charged Higgs bosons decrease with increasing mass m_+ and vice versa. Our choice $\tan\beta = 0.7$ and $m_+ > 720$ GeV in our three 2HDM scenarios falls into the allowed parameter range which is determined by comparing experimental data with 2HDM predictions [37–39].

The allowed parameters of 2HDM are also restricted by the experimental values of the oblique electroweak parameters. The general expressions for the oblique parameters S , T , and U in 2HDM and discussion of resulting constraints can be found in [6, 47–49]. As we have chosen ϕ_1 to be SM-like, ϕ_2, ϕ_3 and H^\pm to be heavy, and the mixing angles such that the couplings of ϕ_2, ϕ_3 to the weak gauge bosons are suppressed, our scenarios are compatible with the constraints from electroweak precision measurements.

The experimental upper limits on the electric dipole moments of the neutron [50] and the electron [51] put limits on the angles associated with Higgs sector CP -violation in 2HDM. Our choice of Higgs mixing angles (14) in the CP -violating scenario 3 which implies the Higgs couplings given Table 5 and our choice of Higgs boson masses (15) lies within the allowed parameter range of CP -violating 2HDM without approximate Z_2 symmetry as derived, for instance, in [35].

4. Theoretical predictions beyond the QCD Born approximation

As mentioned in the introduction the aim of this article is to study, within the type-II two-Higgs-doublet model, the resonant production of heavy neutral Higgs bosons and their decay into $t\bar{t}$,

$$pp \rightarrow \phi_{2,3} \rightarrow t\bar{t}X, \quad (16)$$

including the nonresonant SM $t\bar{t}$ background

$$pp \rightarrow t\bar{t}X \quad (17)$$

and the interference of the resonant and nonresonant amplitudes. Specifically, we consider the three scenarios introduced in Sec. 3 and derive predictions for the cross section and distributions including all relevant NLO QCD corrections.

4.1. Setup and leading-order results

In order to set up our conventions and introduce some abbreviations we start with a short review of the leading-order results. For a detailed discussion we refer to Refs. [17, 19] and Ref. [24] where detector effects have been included in the simulation. As usual, the hadronic cross section is calculated from the partonic cross section through a convolution with the parton distribution functions (PDF),

$$d\sigma_{pp \rightarrow t\bar{t}X} = \sum_{i,j} \int dx_i dx_j F_{i/p}(x_i, \mu_f) F_{j/p}(x_j, \mu_f) d\hat{\sigma}_{ij \rightarrow t\bar{t}X}(x_i P_1, x_j P_2, \mu_f, \mu_r), \quad (18)$$

where the $F_{i/p}(x, \mu_f)$ denote the PDF, μ_f and μ_r are the factorization and renormalization scales, and $\hat{\sigma}_{ij \rightarrow t\bar{t}X}$ denote the partonic cross sections. The sum runs over all parton configurations contributing to top-quark pair production. Within QCD the dominant contributions are

due to gluon fusion ($gg \rightarrow t\bar{t}$) and quark-antiquark annihilation ($q\bar{q} \rightarrow t\bar{t}$). The leading-order Feynman diagrams are shown in Fig. 1. The relative contributions of these two processes to

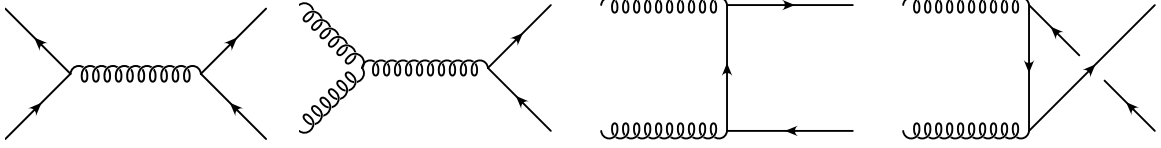


Figure 1: Dominant SM processes contributing to top-quark pair production.

(18) depend on the energy scale, with the contribution from gluon fusion dominating at low energies [52]. In Fig. 2 the additional contribution due to the s -channel exchange of a Higgs boson ϕ_i is shown. In principle, all quarks contribute in the fermion triangles. However in the scenarios considered here we have set $\tan\beta = 0.7$. Thus the bottom Yukawa coupling is not enhanced (as would be the case in scenarios with $\tan\beta \gg 1$). That is why in these scenarios the bottom loop contribution is more suppressed than in the SM with respect to the contribution from the top-quark loop. Contributions from quarks lighter than the b quark are even smaller. Hence we can safely neglect all quark flavor contributions to the triangle which are lighter than the top quark. As we consider here an extended Higgs sector, we have to sum over the (neutral) Higgs bosons ϕ_1, ϕ_2 , and ϕ_3 . We identify ϕ_1 with the SM Higgs boson which con-

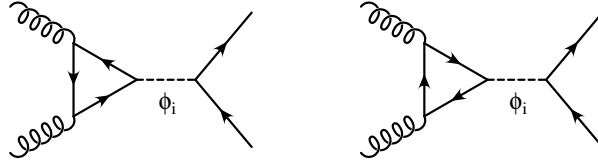


Figure 2: s -channel Higgs boson contribution to top-quark pair production.

tributes to the nonresonant background (17). Since we are mainly interested in the resonant production of the heavy Higgs bosons ϕ_2 and ϕ_3 we take at leading order only the contribution from the diagrams shown in Fig. 2 into account and neglect nonresonant Yukawa corrections due to $\phi_{2,3}$ exchange.

For $gg \rightarrow t\bar{t}$ the scattering amplitude may be written as

$$\mathcal{A} = \mathcal{A}_{\text{QCD}}^{(0)} + \sum_i \mathcal{A}_{\phi_i}^{(0)} \quad (19)$$

and the partonic cross section can be calculated using

$$d\sigma_{gg \rightarrow t\bar{t}} = \frac{1}{32\pi} \frac{\beta_t}{s} |\overline{\mathcal{A}}|^2 d\cos(\theta), \quad (20)$$

where s denotes the partonic center-of-mass energy squared, $\cos(\theta)$ is the cosine of the scattering angle in the parton center-of-mass system (cms),

$$\beta_t = \sqrt{1 - \frac{4m_t^2}{s}} \quad (21)$$

is the velocity of the top quark in the partonic cms, and m_t denotes the top-quark mass renormalized in the on-shell scheme. We overline the squared matrix element in Eq. (20) to indicate that it is averaged/summed over the incoming/outgoing spin and color degrees of freedom. Squaring the amplitude for $gg \rightarrow t\bar{t}$ leads to

$$|\overline{\mathcal{A}_{\text{QCD}}^{(0)}}|^2 + 2 \sum_i \text{Re}(\overline{\mathcal{A}_{\text{QCD}}^{(0)}} \overline{\mathcal{A}_{\phi_i}^{(0)*}}) + 2 \sum_{i>j} \text{Re}(\overline{\mathcal{A}_{\phi_i}^{(0)}} \overline{\mathcal{A}_{\phi_j}^{(0)*}}) + \sum_i |\overline{\mathcal{A}_{\phi_i}^{(0)}}|^2. \quad (22)$$

For the scenarios 1 – 3 discussed in Sec. 3 sizeable effects due to the extended Higgs sector can only be expected well above the threshold for top-quark pair production in the vicinity of the respective resonances ϕ_2, ϕ_3 . (At these energies, the contribution of the SM-like Higgs boson ϕ_1 is tiny and will, in fact, be incorporated in the following sections into the nonresonant background contributions.) The expression for the pure QCD matrix element squared $|\overline{\mathcal{A}_{\text{QCD}}^{(0)}}|^2$ in Eq. (22) can be found in Refs. [53, 54]. For the two heavy Higgs bosons the interference with the QCD amplitude reads

$$2 \sum_{i=2,3} \overline{\text{Re}(\mathcal{A}_{\text{QCD}}^{(0)} \mathcal{A}_{\phi_i}^{(0)*})} = -\frac{16\pi\alpha_s m_t^2}{C_A C_F v} \frac{s}{1 - \beta_t^2 z^2} \sum_{i=2,3} \left[a_{it} \beta_t^2 \text{Re}(P_i(s) \mathcal{F}_i^S) - 2b_{it} \text{Re}(P_i(s) \mathcal{F}_i^P) \right], \quad (23)$$

with the propagator of the Higgs boson ϕ_i defined by

$$P_i(s) = \frac{1}{s - m_i^2 + im_i \Gamma_i}, \quad (24)$$

and the s dependent vertex factors given by

$$\mathcal{F}_i^S = -\frac{\alpha_s a_{it}}{8\pi v} \tau [(1 - \tau)f(\tau) - 1], \quad (25)$$

$$\mathcal{F}_i^P = \frac{\alpha_s b_{it}}{16\pi v} \tau f(\tau), \quad (26)$$

where

$$\tau = 1 - \beta_t^2 = \frac{4m_t^2}{s}. \quad (27)$$

The loop function f is given by

$$f(\tau) = \begin{cases} \frac{1}{4} \left[\ln\left(\frac{1 + \sqrt{1 - \tau}}{1 - \sqrt{1 - \tau}}\right) - i\pi \right]^2 & \tau < 1 \\ -\arcsin^2\left(\sqrt{\frac{1}{\tau}}\right) & \tau \geq 1 \end{cases}. \quad (28)$$

The a_{it} (b_{it}) denote the reduced (pseudo-)scalar Yukawa couplings defined in Sec. 3. The Γ_i are the constant widths of the ϕ_i as given in Sec. 3. $\alpha_s \equiv \alpha_s(\mu_r)$ is the coupling constant of the strong interaction evaluated at the renormalization scale μ_r . C_A and C_F are the Casimir invariants of the SU(N) gauge group ($N = 3$ for QCD),

$$C_A = N, \quad C_F = \frac{1}{2N}(N^2 - 1), \quad (29)$$

and z is the cosine of the scattering angle of the top quark defined in the parton cms,

$$z = \cos(\theta_t). \quad (30)$$

The two remaining contributions in Eq. (22) read

$$\sum_{i=2,3} \overline{|\mathcal{A}_{\phi_i}^{(0)}|^2} = \frac{2}{C_F} \frac{m_t^2}{v^2} s^3 \sum_{i=2,3} |P_i(s)|^2 (|\mathcal{F}_i^S|^2 + 4|\mathcal{F}_i^P|^2) (a_{it}^2 \beta_t^2 + b_{it}^2), \quad (31)$$

$$2\text{Re}(\overline{\mathcal{A}_{\phi_2}^{(0)} \mathcal{A}_{\phi_3}^{(0)*}}) = \frac{4}{C_F} \frac{m_t^2}{v^2} s^3 \text{Re} \left[P_2(s) P_3(s)^* (\mathcal{F}_2^S \mathcal{F}_3^{S*} + 4\mathcal{F}_2^P \mathcal{F}_3^{P*}) \right] (a_{2t} a_{3t} \beta_t^2 + b_{2t} b_{3t}). \quad (32)$$

The interference term (32) is nonzero only in CP -violating scenarios, where ϕ_2, ϕ_3 have both scalar and pseudoscalar components. Although a detailed phenomenological discussion including higher order corrections will be presented in Sec. 5 it is useful to study the size of the different contributions (22) to the LO differential cross section (18). The cross section for top-quark pair production differential in the invariant mass $M_{t\bar{t}}$ of the top-quark pair is shown in Fig. 3 for scenario 3. As anticipated, sizeable effects due to the extended Higgs sector are only visible in the vicinity of the resonances. A distinctive peak-dip structure, which is due to the interference of the Higgs signal with the QCD background amplitude, is visible for the lighter of the two heavy Higgs resonances (which is ϕ_2 in scenario 3). The heavier Higgs boson produces a similar peak-dip structure which is, however, less pronounced and hidden by the effect of the lighter resonance. As a consequence of the peak-dip structure the contribution of the extended Higgs sector to the total $t\bar{t}$ cross section is very small and below the currently attainable experimental accuracy. The effect can be enhanced by introducing a cut on $M_{t\bar{t}}$ and evaluating the cross sections in the regions $2m_t < M_{t\bar{t}} < 480$ GeV and $M_{t\bar{t}} > 480$ GeV. However, even in this case the effects are only at the level of a few percent. Qualitatively similar results are obtained for scenarios 1 and 2.

Contrary to scenarios 1 and 2 the ϕ_2 - ϕ_3 interference term is nonzero in scenario 3. As shown in Fig. 3 this term is small compared to the other contributions; it is less than 0.4 per mill with respect to the QCD background in each $M_{t\bar{t}}$ bin. There are two reasons for this interference to be so small. First, in scenario 3 the Higgs boson mass separation $\Delta m = m_3 - m_2 > \Gamma_2 + \Gamma_3$ leads to a suppression caused by the product of the two Higgs boson propagators in Eq. (32), while in the case $\Delta m = 0$ there is no such suppression. This behavior is displayed in Fig. 4, where the red curve shows the relative contribution of the ϕ_2 - ϕ_3 interference term to the LO hadronic $pp \rightarrow \phi_2, \phi_3 \rightarrow t\bar{t}$ cross section without the QCD background as a function of the mass separation $\Delta m = m_3 - m_2$. Second, even in the case $\Delta m = 0$ the ϕ_2 - ϕ_3 interference term is still small (about 4% compared to the Higgs-only cross section). This is the result of our choice

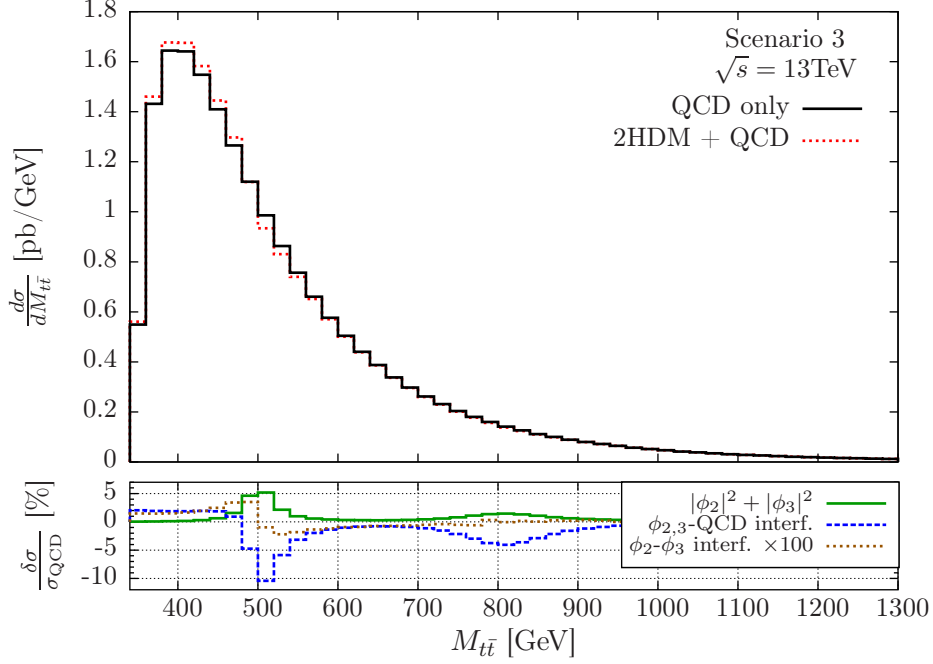


Figure 3: Impact of different contributions to the hadronic differential cross section $d\sigma/dM_{t\bar{t}}$ at leading order. Upper pane: The solid black curve shows the QCD background and the dotted red curve displays the sum of QCD background, 2HDM contribution and the interference term. Lower pane: Relative contributions with respect to the QCD background. The solid green curve shows the sum of the contributions from ϕ_2 and ϕ_3 , the dashed blue curve depicts the interference of the ϕ_2, ϕ_3 production amplitudes with the QCD background, and the dotted brown curve the ϕ_2 - ϕ_3 interference (multiplied with a factor 100 for better visibility).

of parameters for scenario 3, which leads to Yukawa couplings with opposite signs. This is in turn responsible for cancellations in Eq. (32) and renders the interference term small. The blue curve in Fig. 4 shows in addition the behavior of this interference term as a function of the Higgs mass separation using an additional cut, namely $m_2 - 150 \text{ GeV} \leq M_{t\bar{t}} \leq m_2$. This cut enhances the ϕ_2 - ϕ_3 interference because it prevents the partial cancellation due to the peak-dip structure which is also present in this interference term. We apply similar cuts in the NLO analysis presented below. Even with this cut the interference contribution Eq. (32) is small compared to the total Higgs boson contributions to the $t\bar{t}$ cross section and can be safely neglected in phenomenological applications.

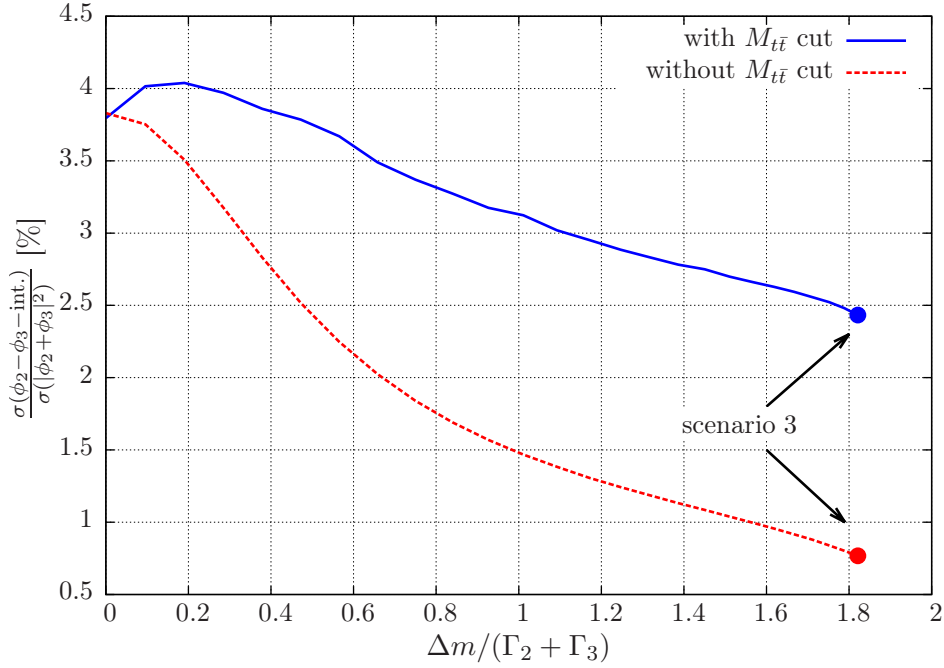


Figure 4: Relative contribution of the ϕ_2 - ϕ_3 -interference term (32) with respect to the total hadronic $pp \rightarrow \phi_2, \phi_3 \rightarrow t\bar{t}$ cross section without QCD background as a function of the mass separation $\Delta m = m_3 - m_2$ normalized to $\Gamma_2 + \Gamma_3$. The parameters used for this plot correspond to those of scenario 3 except for the masses and widths of ϕ_2 and ϕ_3 which have been varied accordingly. The end of each curve corresponds exactly to scenario 3 with $m_2 = 500 \text{ GeV}$, $m_3 = 800 \text{ GeV}$ and corresponding widths as given in Table 6.

In order to find or put limits on heavy Higgs boson production and decay to $t\bar{t}$ the experimental analysis must focus on the resonance region. Since the mass(es) of the heavy resonance(s) is (are) not known beforehand, an analysis with a sliding $M_{t\bar{t}}$ window combined with a sideband analysis should be applied. From the theoretical point of view NLO corrections are required to provide reliable predictions in the vicinity of the resonances. The evaluation of the NLO corrections will be discussed in the next subsection.

Besides we remark that, depending on the mass, couplings and width of the heavy Higgs resonance, a pure dip rather than a peak dip may show up in the $M_{t\bar{t}}$ spectrum, or even a complete washout of the resonance signal can occur. For a recent analysis, see Ref. [25]. For the parameter scenarios described in Sec. 3 the lighter of the two heavy Higgs resonances produces always a peak-dip structure in the $M_{t\bar{t}}$ distribution; see Sec. 5.

4.2. Next-to-leading order QCD corrections

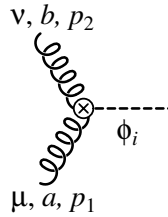
For the calculation of the NLO QCD corrections to the process in Eq. (16) we apply two approximations. First, as far as the Higgs coupling to the gluons is concerned, we work in the heavy top-quark limit. Second, we take advantage of the fact that the theoretical predictions are only required in the vicinity of the resonances because the experimental analysis will focus on this region. This allows us to work in the pole approximation, keeping only contributions that are resonant in the intermediate Higgs boson(s). This is consistent with our approach to work at leading order in the Yukawa couplings. The heavy Higgs resonances are described by a Breit-Wigner propagator with constant width. In our approach this amounts to using the so-called complex mass scheme [55–57], as outlined in Appendix A.

In order to fix our conventions we briefly review the approximations in the following.

Effective theory approach: In the heavy top-quark limit the triangles shown in Fig. 2 are shrunk to an effective vertex.³ Relying on Lorentz covariance and gauge invariance, the effective vertex can be described within an effective field theory approach with the relevant contribution to the Lagrangian given by

$$\mathcal{L}_{\text{eff}} = \sum_{j=2}^3 \left[f_{Sj} G_{\mu\nu}^a G_a^{\mu\nu} + f_{Pj} \epsilon_{\mu\nu\alpha\beta} G_a^{\mu\nu} G_a^{\alpha\beta} \right] \phi_j, \quad (33)$$

where f_{Sj} and f_{Pj} are the Wilson coefficients for the coupling of the CP -even and CP -odd component of the Higgs boson ϕ_j to gluons. The effective Lagrangian leads to the following Feynman rules ($g_s = \sqrt{4\pi\alpha_s}$)



$$= -4i\delta^{ab} \left[f_{Sj} \left(g_{\mu\nu} (p_1 \cdot p_2) - p_{2\mu} p_{1\nu} \right) - 2f_{Pj} \epsilon_{\mu\nu\rho\sigma} p_1^\rho p_2^\sigma \right], \quad (34)$$

³The virtual NLO QCD corrections for scalar and pseudoscalar Higgs-boson production in gluon fusion were calculated for arbitrary quark masses in Ref. [58].

$$\begin{aligned}
& \text{Diagram} = 4g_s f^{abc} \left\{ f_{Sj} \left[g_{\mu\nu}(p_1 - p_2)_\rho + g_{\nu\rho}(p_2 - p_3)_\mu + g_{\rho\mu}(p_3 - p_1)_\nu \right] \right. \\
& \quad \left. - 2f_{Pj}(p_1 + p_2 + p_3)^\alpha \epsilon_{\alpha\mu\nu\rho} \right\}. \tag{35}
\end{aligned}$$

The momenta are taken to be incoming and we use the convention $\epsilon_{0123} = +1$. The Lagrangian \mathcal{L}_{eff} contains also an effective $gggg\phi_j$ coupling, which is however not needed at the order of perturbation theory in which we are working. The effective couplings f_{Sj} and f_{Pj} can be further expanded in powers of α_s :

$$f_{Sj} = \frac{\alpha_s}{\pi} \left(f_{Sj}^{(0)} + \frac{\alpha_s}{\pi} f_{Sj}^{(1)} + \dots \right), \quad f_{Pj} = \frac{\alpha_s}{\pi} \left(f_{Pj}^{(0)} + \frac{\alpha_s}{\pi} f_{Pj}^{(1)} + \dots \right). \tag{36}$$

Comparing the results obtained in the full theory as presented in the previous subsection with the results in the effective theory approach, it is straightforward to obtain the well-known result:

$$\frac{\alpha_s}{\pi} f_{Sj}^{(0)} = \lim_{m_t \rightarrow \infty} \mathcal{F}_j^S = \frac{\alpha_s}{\pi} \frac{a_{jt}}{12v}, \tag{37}$$

$$\frac{\alpha_s}{\pi} f_{Pj}^{(0)} = \lim_{m_t \rightarrow \infty} \mathcal{F}_j^P = -\frac{\alpha_s}{\pi} \frac{b_{jt}}{16v}. \tag{38}$$

Using the expressions from Ref. [59–62] adapted to our conventions we get for $f_{Sj}^{(1)}$ and $f_{Pj}^{(1)}$:

$$f_{Sj}^{(1)} = \frac{(4\pi)^\epsilon}{\Gamma(1-\epsilon)} \frac{a_{jt}}{12v} \left(\frac{11}{4} - \frac{\beta_0}{\epsilon} \right) = \frac{(4\pi)^\epsilon}{\Gamma(1-\epsilon)} f_{Sj}^{(0)} \left(\frac{11}{4} - \frac{\beta_0}{\epsilon} \right), \tag{39}$$

$$f_{Pj}^{(1)} = \frac{(4\pi)^\epsilon}{\Gamma(1-\epsilon)} \frac{b_{jt}}{16v} \frac{\beta_0}{\epsilon} = -\frac{(4\pi)^\epsilon}{\Gamma(1-\epsilon)} f_{Pj}^{(0)} \frac{\beta_0}{\epsilon}, \tag{40}$$

where $\epsilon = (4-d)/2$ is the dimensional regulator working in d dimensions, and

$$\beta_0 = \frac{1}{2} \left(\frac{11}{6} C_A - \frac{2}{3} T_R N_F \right) \tag{41}$$

denotes the leading coefficient of the QCD β -function with N_F being the number of massless quark flavors and $T_R = 1/2$. One may question the validity of the heavy top-quark limit given that we apply the effective theory approach above the threshold of top-quark pair production. Since the effective theory approach has been shown to provide also reliable estimates for energies well above its naive domain of validity—if the full leading-order result is kept and an appropriate reweighting is performed [29]—we believe that reliable estimates of the NLO corrections can be obtained within this approximation. We outline our reweighting method adapted from Ref. [29] at the end of this section.

Pole contribution and soft gluon approximation: As sizeable effects of the extended Higgs sector can be expected only in the heavy Higgs boson resonance region it is sufficient to restrict the theoretical predictions to $M_{t\bar{t}}$ intervals around the Higgs boson masses. This can be achieved by the pole approximation where only the contributions enhanced by a resonant propagator are kept. For Higgs propagators appearing within loop diagrams the soft gluon

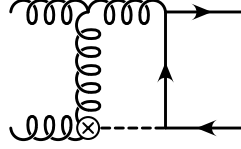


Figure 5: Diagram to be calculated in the soft gluon approximation.

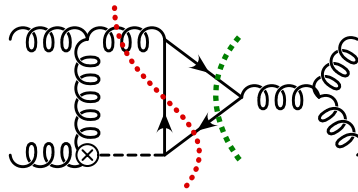


Figure 6: Virtual (green dashed) and real (red dotted) contributions which cancel in the soft gluon approximation.

approximation can be used to extract the leading pole contribution. Taking as an example the diagram shown in Fig. 5 it is clear that a resonant contribution at $M_{t\bar{t}} \approx m_i$ is only possible if the additional gluon in the loop is soft. This is the essence of the soft gluon approximation in which the integrand of the loop integral is approximated by the contribution from soft gluons. Note that the loop integration is not restricted within this approximation. For more details we refer to Refs. [63–66]. Evidently, the same approximation has to be applied also to the real corrections. In fact, the virtual corrections alone are infrared divergent because the soft gluon is coupled to external lines. Only the sum of the virtual and real corrections yields a finite result. In the soft gluon limit the amplitudes simplify significantly and it turns out that the appropriate real corrections completely cancel the corresponding virtual contributions once sufficiently inclusive observables are studied. An example of this cancellation is illustrated in Fig. 6. This was checked for the various contributions on a case by case study. More details about the example shown in Fig. 6 are given in Appendix B. The corrections of the type displayed in Figs. 5–6 are also called nonfactorizable corrections because the gluon radiation connects Higgs boson production and decay to $t\bar{t}$. We also stress that gauge invariance is only guaranteed if the soft gluon approximation is consistently applied.

After these introductory remarks we now briefly summarize the various terms that contribute, within the aforementioned approximations, to resonant ϕ_j production and interference with the nonresonant $t\bar{t}$ amplitudes at NLO QCD, i.e., at order α_s^3 . In Fig. 7 the factorizing QCD

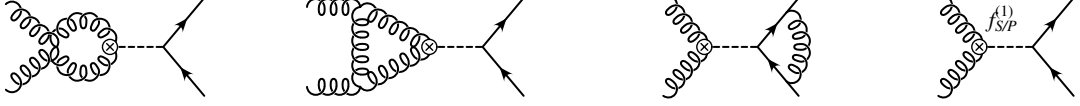


Figure 7: QCD corrections to top-quark pair production via resonant Higgs exchange.

corrections for top-quark pair production through Higgs exchange are shown and we do not display diagrams that vanish in dimensional regularization. Denoting the amplitude for this contribution with $\mathcal{A}_{\phi_i}^{(1)}$ and the QCD corrections to nonresonant top-quark pair production (without any Higgs contribution) with $\mathcal{A}_{\text{QCD}}^{(1)}$, the virtual corrections to the squared matrix element read

$$\sum_{i,j} 2\text{Re}\left(\mathcal{A}_{\phi_i}^{(1)}\mathcal{A}_{\phi_j}^{(0)*}\right) + \sum_i 2\text{Re}\left(\mathcal{A}_{\phi_i}^{(1)}\mathcal{A}_{\text{QCD}}^{(0)*}\right) + \sum_i 2\text{Re}\left(\mathcal{A}_{\text{QCD}}^{(1)}\mathcal{A}_{\phi_i}^{(0)*}\right). \quad (42)$$

We refrain from discussing the NLO QCD corrections to $t\bar{t}$ production here, because they have been known for a long time [53, 54, 67–70]. (In [69, 70] the full spin dependence of the top quarks is kept.) After renormalization the virtual corrections are ultraviolet (UV) finite. However, they still contain infrared (IR) singularities which are canceled only after the inclusion of the real corrections. Sample diagrams for $gg \rightarrow \phi_i \rightarrow t\bar{t}g$ are shown in Fig. 8. The square of this amplitude cancels the IR singularities in $2\text{Re}\left(\mathcal{A}_{\phi_i}^{(1)}\mathcal{A}_{\phi_j}^{(0)*}\right)$. Because of the

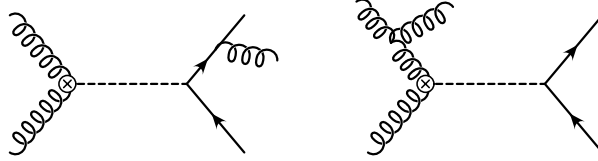


Figure 8: Sample diagrams for initial and final state real corrections to the process $gg \rightarrow \phi_{2,3} \rightarrow t\bar{t}$.

color structure there is no interference between initial and final state radiation in this case. The amplitude for $gg \rightarrow \phi_i \rightarrow t\bar{t}g$ interferes also with the QCD amplitude $gg \rightarrow t\bar{t}g$. This contribution cancels the IR singularities in $\sum_i 2\text{Re}\left(\mathcal{A}_{\phi_i}^{(1)}\mathcal{A}_{\text{QCD}}^{(0)*}\right)$ and $\sum_i 2\text{Re}\left(\mathcal{A}_{\text{QCD}}^{(1)}\mathcal{A}_{\phi_i}^{(0)*}\right)$. We stress that the contribution to be combined with $\sum_i 2\text{Re}\left(\mathcal{A}_{\phi_i}^{(1)}\mathcal{A}_{\text{QCD}}^{(0)*}\right)$ is evaluated using the soft gluon approximation.

At order α_s^3 heavy Higgs bosons can also be produced by $q\bar{q}$ annihilation with an amplitude that is not suppressed by light quark Yukawa couplings. The respective Feynman diagram for $q\bar{q} \rightarrow t\bar{t}g$ is shown in Fig. 9. Besides the square of this amplitude also the interference with the QCD amplitude for $q\bar{q} \rightarrow t\bar{t}g$ contributes. Both contributions are free of IR singularities.

In addition, resonant heavy Higgs boson production and decay to $t\bar{t}$ occurs also by (anti)quark gluon fusion, $qg \rightarrow t\bar{t}q$ and $g\bar{q} \rightarrow t\bar{t}\bar{q}$. The corresponding amplitudes are obtained from the

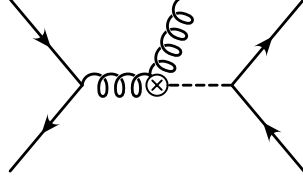


Figure 9: Resonant heavy Higgs boson production in $q\bar{q} \rightarrow t\bar{t}g$.

amplitude depicted in Fig. 9 by crossing. The square of the amplitude with the intermediate Higgs bosons and the interference with the respective QCD amplitude lead to double and single resonant terms. Contrary to the $q\bar{q}$ case both contributions suffer from initial state singularities.

Some technical aspects: The calculation of the NLO corrections described above is conceptually straightforward. Since the full results are rather lengthy we briefly outline the calculation and show explicit results for some illustrative examples only. As far as the virtual corrections are concerned we employ the Passarino-Veltman reduction [71] to reduce the one-loop tensor integrals to scalar integrals. Including the contribution from UV renormalization we obtain for example for the interference of the diagrams shown in Fig. 7 and the leading-order Higgs boson exchange diagrams

$$\begin{aligned}
\sum_{i,j} \overline{2\text{Re}(\mathcal{A}_{\phi_i}^{(1)} \mathcal{A}_{\phi_j}^{(0)*})} &= \frac{\alpha_s}{\pi} \left\{ -\frac{(4\pi)^\epsilon}{\Gamma(1-\epsilon)} \left\{ \text{Re} \left[\left(\frac{\mu^2}{-s-i0} \right)^\epsilon \right] \frac{C_A}{\epsilon^2} + \frac{2\beta_0}{\epsilon} \right\} \mathcal{B} \right. \\
&+ \left(\frac{4\pi\mu^2}{m_t^2} \right)^\epsilon \Gamma(1+\epsilon) C_F \frac{1}{\epsilon} \text{Re}(a_{-1}) \mathcal{B} \\
&+ \frac{11}{2} \mathcal{B}|_{f_P=0} + 2C_A \mathcal{B}|_{f_S=0} \\
&\left. + C_F \left[\text{Re}(a_0) \mathcal{B}|_{b_t=0} + \text{Re}(\bar{a}_0) \mathcal{B}|_{a_t=0} \right] + \mathcal{O}(\epsilon) \right\}, \quad (43)
\end{aligned}$$

where \mathcal{B} denotes the contribution from

$$\sum_{i=2,3} \overline{|\mathcal{A}_{\phi_i}^{(0)}|^2} + \overline{2\text{Re}(\mathcal{A}_{\phi_2}^{(0)} \mathcal{A}_{\phi_3}^{(0)*})}$$

evaluated in the heavy top-quark limit:

$$\begin{aligned}
\mathcal{B} &= \frac{2}{C_F} \left(\frac{\alpha_s}{\pi} \right)^2 \frac{m_t^2}{v^2} s^3 \left\{ \sum_{i=2,3} |P_i(s)|^2 (|f_{S_i}^{(0)}|^2 + 4|f_{P_i}^{(0)}|^2) (a_{it}^2 \beta_t^2 + b_{it}^2) \right. \\
&\left. + 2\text{Re} \left[P_2(s) P_3(s)^* (f_{S_2}^{(0)} f_{S_3}^{(0)*} + 4f_{P_2}^{(0)} f_{P_3}^{(0)*}) \right] (a_{2t} a_{3t} \beta_t^2 + b_{2t} b_{3t}) \right\}. \quad (44)
\end{aligned}$$

The coefficients a_{-1} , a_0 and \bar{a}_0 are related to the one-loop $\phi_j \rightarrow t\bar{t}$ form factor and can be taken for example from Ref. [72]. The poles in the dimensional regulator ϵ are due to IR singularities. Note that we keep the polarization of the incoming gluons in four dimensions. As a consequence \mathcal{B} does not depend on ϵ . The IR singularities are handled with the Catani-Seymour dipole subtraction [73, 74]. In this formalism local counterterms are added to the real corrections such that on the one hand the soft and collinear singularities are canceled point-wise in phase space and, on the other hand, the subtraction is simple enough to be integrated analytically over the d -dimensional phase space of the unobserved parton. The cross section reads schematically [73]:

$$\begin{aligned}
\sigma^{\text{NLO}} &= \sigma^{\text{NLO}\{m+1\}}(p) + \sigma^{\text{NLO}\{m\}}(p) + \int_0^1 dx d\hat{\sigma}^{\text{NLO}\{m\}}(x; xp) \\
&= \int_{m+1} \left[\left(\sigma^{\text{R}}(p) \right)_{\epsilon=0} - \left(\sum_{\text{dipoles}} d\sigma^{\text{B}}(p) \otimes (dV_{\text{dipole}} + dV'_{\text{dipole}}) \right)_{\epsilon=0} \right] \\
&+ \int_m \left[d\sigma^{\text{V}}(p) + d\sigma^{\text{B}}(p) \otimes \mathbf{I} \right]_{\epsilon=0} + \int_0^1 dx \int_m \left[d\sigma^{\text{B}}(xp) \otimes (\mathbf{K} + \mathbf{P})(x) \right]. \quad (45)
\end{aligned}$$

Here σ^{B} , σ^{V} , and σ^{R} denote the Born cross section and the contributions from the virtual and real corrections, respectively. Since the real corrections combined with the subtraction terms are finite, they can be evaluated numerically in four dimensions. The singularities are thus made manifest in the integrated subtraction terms which are added back [last line in Eq. (45)]. The subtraction term to be combined with the real corrections is constructed as a sum of individual dipoles:

$$\sum_{\text{dipoles}} d\sigma^{\text{B}}(p) \otimes (dV_{\text{dipole}} + dV'_{\text{dipole}}).$$

The analytically integrated dipoles are collected in the operators \mathbf{I} , \mathbf{K} , and \mathbf{P} which may introduce correlations in spin and color. Combining for the case at hand the virtual corrections with the contribution from the \mathbf{I} operator an IR finite result is obtained:

$$\begin{aligned}
d\sigma_{\text{V}} + d\sigma_{\mathbf{I}} &= \frac{1}{32\pi} \frac{\alpha_s \beta_t}{\pi s} \left\{ \left[2\beta_0 + \frac{67}{18} C_A - \frac{10}{9} N_F T_R \right. \right. \\
&+ C_F \left(3 - \frac{\beta_t^2 + 6\beta_t + 1}{12\beta_t} \pi^2 - \frac{1 + \beta_t^2}{4\beta_t} \ln^2 y - \frac{1 + \beta_t^2}{2\beta_t} \ln \left(\frac{1 + \beta_t^2}{2} \right) \ln(y) \right. \\
&+ \left. \left. \left(\frac{1 + \beta_t^2}{2\beta_t} \ln(y) + \frac{3}{2} \right) \ln \left(\frac{1 - \beta_t^2}{2(1 + \beta_t^2)} \right) + \mathcal{V}_q^{(\text{NS})} \right] + 2\beta_0 \ln \left(\frac{\mu^2}{s} \right) \right] \mathcal{B} \\
&+ 2C_A \mathcal{B}|_{f_S=0} + \frac{11}{2} \mathcal{B}|_{f_S=0} \\
&+ \left. C_F \left[\text{Re}(a_0) \mathcal{B}|_{b_t=0} + \text{Re}(\bar{a}_0) \mathcal{B}|_{a_t=0} \right] \right\} d\cos(\theta) \quad (46)
\end{aligned}$$

with

$$\begin{aligned}
\mathcal{V}_q^{(\text{NS})} &= \frac{3}{2} \ln\left(\frac{1}{2}(1+\beta_t^2)\right) \\
&+ \frac{1+\beta_t^2}{2\beta_t} \left(2\ln(y) \ln\left(\frac{2(1+\beta_t^2)}{(1+\beta_t)^2}\right) + 2\text{Li}_2(y^2) - 2\text{Li}_2\left(\frac{2\beta_t}{1+\beta_t}\right) - \frac{\pi^2}{6} \right) \\
&+ \ln\left(1 - \frac{1}{2}\sqrt{1-\beta_t^2}\right) - 2\ln\left(1 - \sqrt{1-\beta_t^2}\right) - \frac{1-\beta_t^2}{1+\beta_t^2} \ln\left(\frac{\sqrt{1-\beta_t^2}}{2-\sqrt{1-\beta_t^2}}\right) \\
&- \frac{\sqrt{1-\beta_t^2}}{2-\sqrt{1-\beta_t^2}} + 2\frac{(1-\sqrt{1-\beta_t^2}-\beta_t^2)}{1+\beta_t^2} + \frac{\pi^2}{2}
\end{aligned} \tag{47}$$

and

$$y = \frac{1-\beta_t}{1+\beta_t}. \tag{48}$$

The sum of the contributions from the integrated dipoles responsible for initial state singularities and the QCD factorization reads

$$\begin{aligned}
d\sigma_{\mathbf{KP}} &= \int_0^1 dx \int_m \left[d\sigma^{\text{B}}(xp) \otimes (\mathbf{K} + \mathbf{P})(x) \right] \\
&= \frac{\alpha_s}{\pi} \int_0^1 dx \int d\Pi_2 \left\{ \overline{K}^{gg}(x) - K_{\text{F.S.}}^{gg}(x) + \widetilde{K}^{gg}(x) - P^{gg}(x) \ln\left(\frac{\mu_F^2}{xs}\right) \right\} \mathcal{B}(xs).
\end{aligned} \tag{49}$$

In the evaluation of $\mathcal{B}(xs)$ the partonic center-of-mass energy squared is set to xs . Since we factorize the initial state singularities in the $\overline{\text{MS}}$ scheme the contribution $K_{\text{F.S.}}^{gg}(x)$ encoding the scheme dependence for schemes different from the $\overline{\text{MS}}$ scheme is zero. For the definition of the remaining contributions we refer to Ref. [73].

For the real corrections very short expressions can be derived for the squared Higgs boson contribution. In the reaction

$$g(p_1) + g(p_2) \rightarrow t(k_1) + \bar{t}(k_2) + g(q) \tag{50}$$

the $t\bar{t}$ pair is produced in a color singlet state. Therefore, the squared matrix element is given by an incoherent sum of two terms associated with gluon radiation from the initial and final state. We find

$$\begin{aligned}
\overline{|\mathcal{A}(gg \xrightarrow{\phi_2, \phi_3} t\bar{t}g)|_{\text{ISR}}^2} &= \frac{16\alpha_s^3 C_A m_t^2 (s+t+u)^4 + s^4 + t^4 + u^4}{\pi C_F v^2 stu} \\
&\times \left\{ \sum_{j=2,3} \left((f_{Sj}^{(0)})^2 + 4(f_{Pj}^{(0)})^2 \right) (-a_{jt}^2 t_{12} + b_{jt}^2 s_{12}) |P_j(s_{12})|^2 \right. \\
&+ \left. 2(f_{S2}^{(0)} f_{S3}^{(0)} + 4f_{P2}^{(0)} f_{P3}^{(0)}) (-a_{2t} a_{3t} t_{12} + b_{2t} b_{3t} s_{12}) \text{Re}[P_{23}(s_{12})] \right\}
\end{aligned} \tag{51}$$

with

$$s = (p_1 + p_2)^2, \quad t = (p_1 - q)^2, \quad u = (p_2 - q)^2, \quad s_{12} = (k_1 + k_2)^2, \quad t_{12} = (k_1 - k_2)^2, \quad (52)$$

and

$$P_{23}(s) = P_2(s)P_3(s)^*. \quad (53)$$

The contribution from final state gluon radiation reads

$$\begin{aligned} \overline{|\mathcal{A}(gg \xrightarrow{\phi_2, \phi_3} t\bar{t}g)|_{\text{FSR}}^2} &= \frac{16\alpha_s^3 s^2 m_t^2}{\pi s_{13}'^2 s_{23}'^2 v^2} \left\{ \sum_{j=2,3} [(f_{S_j}^{(0)})^2 + 4(f_{P_j}^{(0)})^2] [a_{jt}^2 K_a + b_{jt}^2 K_b] |P_j(s)|^2 \right. \\ &\quad \left. + 2[f_{S_2}^{(0)} f_{S_3}^{(0)} + 4f_{P_2}^{(0)} f_{P_3}^{(0)}] [a_{2t} a_{3t} K_a + b_{2t} b_{3t} K_b] \text{Re}[P_{23}(s)] \right\} \quad (54) \end{aligned}$$

with

$$K_a = 8m_t^4 (s - s_{12})^2 - 2m_t^2 (s(s_{13}' + s_{23}')^2 + 4s_{12}s_{13}'s_{23}') + s_{13}'s_{23}'(s^2 + s_{12}^2), \quad (55)$$

$$K_b = s_{13}'s_{23}'(s^2 + s_{12}^2) - 2m_t^2 s(s - s_{12})^2, \quad (56)$$

and

$$s_{13}' = 2k_1 \cdot q, \quad s_{23}' = 2k_2 \cdot q. \quad (57)$$

For the quark initiated processes

$$q(p_1) + \bar{q}(p_2) \rightarrow t(k_1) + \bar{t}(k_2) + g(q) \quad (58)$$

and

$$q(p_1) + g(p_2) \rightarrow t(k_1) + \bar{t}(k_2) + q(q) \quad (59)$$

the squared amplitudes without the QCD interference are given by

$$\begin{aligned} \overline{|\mathcal{A}(qg \xrightarrow{\phi_2, \phi_3} t\bar{t}q)|^2} &= \frac{16\alpha_s^3 m_t^2 s^2 + u^2}{\pi v^2 - t} \left\{ \sum_{j=2,3} [(f_{S_j}^{(0)})^2 + 4(f_{P_j}^{(0)})^2] (-a_{jt}^2 t_{12} + b_{jt}^2 s_{12}) |P_j(s_{12})|^2 \right. \\ &\quad \left. + 2[f_{S_2}^{(0)} f_{S_3}^{(0)} + 4f_{P_2}^{(0)} f_{P_3}^{(0)}] (-a_{2t} a_{3t} t_{12} + b_{2t} b_{3t} s_{12}) \text{Re}[P_{23}(s_{12})] \right\} \quad (60) \end{aligned}$$

and

$$\begin{aligned} \overline{|\mathcal{A}(q\bar{q} \xrightarrow{\phi_2, \phi_3} t\bar{t}g)|^2} &= \frac{32\alpha_s^3 C_F m_t^2 t^2 + u^2}{\pi v^2 s} \left\{ \sum_{j=2,3} [(f_{S_j}^{(0)})^2 + 4(f_{P_j}^{(0)})^2] (-a_{jt}^2 t_{12} + b_{jt}^2 s_{12}) |P_j(s_{12})|^2 \right. \\ &\quad \left. + 2[f_{S_2}^{(0)} f_{S_3}^{(0)} + 4f_{P_2}^{(0)} f_{P_3}^{(0)}] (-a_{2t} a_{3t} t_{12} + b_{2t} b_{3t} s_{12}) \text{Re}[P_{23}(s_{12})] \right\}. \quad (61) \end{aligned}$$

The interferences of the signal amplitudes with the nonresonant QCD amplitudes produce rather lengthy expressions and we do not reproduce them here. As far as the NLO QCD and

weak corrections to $t\bar{t}$ without contributions from ϕ_2 and ϕ_3 are concerned, we use the results of our previous work [69, 70, 75]. As mentioned above, the (small) contribution from the SM-like Higgs boson $\phi_1(125\text{GeV})$ is part of the order $\alpha_s^2\alpha$ mixed QCD-weak corrections.

As already emphasized at the beginning of this section we apply the large top-quark mass limit for the computation of the NLO QCD corrections to heavy Higgs production. Because we work above the top-quark pair production threshold we use this approximation somewhat beyond its range of validity. However, in Ref. [29] it was shown that the range of application can be extended to $m_\phi > 2m_t$ within rather small uncertainties ($\approx 10\%$), provided the higher order corrections are rescaled by an appropriate K factor. This procedure has been examined for the production of a heavy Higgs boson by gluon fusion in the SM, $pp \rightarrow \phi + X$. In Ref. [29] it was also shown that the main contribution to the QCD NLO corrections is due to soft and collinear gluon radiation which does not resolve the gluon-Higgs coupling. Because the QCD corrections to

$$pp \rightarrow \phi_2, \phi_3 \rightarrow t\bar{t}, \quad (62)$$

especially the factorizing ones, are very similar to those of Higgs production by gluon fusion in the SM, it is well motivated to assume the same behavior with respect to the effective gluon-Higgs couplings that we use. The K-factor method applied to our calculation should therefore lead to reliable results. Compared to the case of inclusive SM Higgs production there is, however, a major difference: the interference with the QCD background. In the following we briefly describe the K-factor method adapted to the situation studied in this article. The total $t\bar{t}$ cross section is written as

$$\sigma_{\text{NLO}} = \sigma_{\text{NLO}}^{\text{QCDW}} + \sigma_{\text{NLO}}^{\text{approx.}}, \quad (63)$$

where $\sigma_{\text{NLO}}^{\text{QCDW}}$ denotes the nonresonant $t\bar{t}$ cross section including the NLO QCD and weak corrections and $\sigma_{\text{NLO}}^{\text{approx.}}$ is the contribution of the heavy Higgs bosons including the interference with the QCD background at NLO. We calculate it as follows⁴:

$$\sigma_{\text{NLO}}^{\text{approx.}} = \sum_{j=2,3} \left(\sigma_{\text{full},j}^{(0)} + \sigma_{\text{full},j,\text{QCD}}^{(0)} + K_j \sigma_{\text{eff},j}^{(1)} + \sigma_{\text{eff},j,\text{QCD}}^{(1)} \right) \quad (64)$$

with

$$K_j = \frac{\sigma_{\text{full},j}^{(0)}}{\sigma_{\text{eff},j}^{(0)}}. \quad (65)$$

Here $\sigma_{\text{full},j}^{(0)}$ denote the leading-order cross sections for

$$pp \rightarrow \phi_j \rightarrow t\bar{t}, \quad (66)$$

and $\sigma_{\text{full},j,\text{QCD}}^{(0)}$ is the interference term of the ϕ_j production amplitude with the background at LO. The full top-quark mass dependence is kept in these two contributions. The terms $\sigma_{\text{eff},j}^{(1)}$ ($\sigma_{\text{eff},j}^{(0)}$) and $\sigma_{\text{eff},j,\text{QCD}}^{(1)}$ represent the NLO (LO) contributions to (66) and the interference with

⁴The formulas are presented here only for the inclusive cross section. However, they can also be applied to each individual bin of a distribution.

the QCD background at NLO, respectively, in the effective theory. The K factor is not applied to the NLO interference term in (64). Using a K factor for this term analogous to Eq. (65),

$$\tilde{K}_j = \frac{\sigma_{\text{full},j,\text{QCD}}^{(0)}}{\sigma_{\text{eff},j,\text{QCD}}^{(0)}}, \quad (67)$$

would lead to a singular behavior whenever $\sigma_{\text{eff},j,\text{QCD}}^{(0)}$ vanishes. This can happen for differential cross sections, e.g. for the $M_{t\bar{t}}$ distribution.

5. Results

For the numerical evaluation of the (differential) cross section discussed in the previous section we use, apart from the 2HDM parameter scenarios introduced in Sec. 3, the following input values. The masses of the top quark (in the on-shell scheme) and of the SM-like Higgs boson ϕ_1 are set to

$$m_t = 173.34 \text{ GeV}, \quad m_1 = 125 \text{ GeV}. \quad (68)$$

We use the following values of the electromagnetic fine structure constant and the gauge boson masses:

$$\alpha = \frac{1}{129}, \quad m_W = 80.385 \text{ GeV}, \quad m_Z = 91.1876 \text{ GeV}. \quad (69)$$

We employ the PDF set CT10nlo [76] which provides also the value of the strong coupling at a scale μ . To estimate the impact of uncalculated higher orders we set the renormalization scale μ_r equal to the factorization scale μ_f ($\mu_f = \mu_r \equiv \mu$) and vary μ by a factor 2 up and down. As the central scale we use

$$\mu_0 = \frac{m_2 + m_3}{4}.$$

This choice is motivated by the choice $\mu_0 = m_H/2$ in the SM case; see, for instance, [77].

In the following we present results for proton-proton collisions at a hadronic center-of-mass energy of $\sqrt{s} = 13 \text{ TeV}$. The $t\bar{t}$ cross section differential in the top-quark pair invariant mass is displayed in Figs. 10–12 for scenarios 1–3. The ratios in the lower panes of these figures show that the corrections with respect to the leading-order Higgs contribution are sizeable but the overall effect of resonant ϕ_2, ϕ_3 production is rather small: In the $M_{t\bar{t}}$ distribution it ranges from below 5% in the CP -violating case with significantly different ϕ_2, ϕ_3 masses (scenario 3) to about 6% in the nearly mass-degenerate CP -conserving case (scenario 1). The effects on the inclusive $t\bar{t}$ cross section are even smaller, as can be seen in Table 7. As a general feature we observe that in all three scenarios the QCD corrections lead to a positive shift in the vicinity of the resonances with respect to the leading-order results. The potential cancellation due to the peak-dip structure, when the resonance region is integrated over, is thus reduced at next-to-leading order.

Because the validity of the predictions is restricted in the pole approximation to the resonant region, we apply $M_{t\bar{t}}$ cuts around the resonance which are indicated as hatched regions in the

lower plots in Figs. 10–12. In order to enhance the signal we divide the $M_{t\bar{t}}$ cuts into two regions. One region is associated with the peak

$$m^* - 150 \text{ GeV} \leq M_{t\bar{t}} \leq m^* \quad (70)$$

and the other one with the dip

$$m^* \leq M_{t\bar{t}} \leq m^* + 150 \text{ GeV}, \quad (71)$$

where m^* is defined as the smallest value of $M_{t\bar{t}}$ where the NLO ratio (red curve in Figs. 10–12) crosses 1. These cuts enhance the signal-to-background ratio because they prevent the partial cancellation due to the peak-dip structure. As already mentioned in the introduction experimental analyses may use a sliding $M_{t\bar{t}}$ window.

Table 7: Inclusive $t\bar{t}$ production cross sections for pp collisions at the hadronic center-of-mass energy of $\sqrt{s} = 13$ TeV in different type-II 2HDM scenarios. σ_{QCDW} denotes the cross section for $pp \rightarrow t\bar{t}$ including NLO QCD and weak corrections, but without contributions from ϕ_2, ϕ_3 . Note that due to our choice of the renormalization and factorization scale $\mu = \mu_0 = (m_2 + m_3)/4$ the cross section σ_{QCDW} depends on the scenario. σ_{2HDM} denotes the cross section for $pp \rightarrow \phi_{2,3} \rightarrow t\bar{t}$ including the interference with the QCD background at NLO QCD. The superscripts (subscripts) correspond to $\mu = \mu_0/2$ ($\mu = 2\mu_0$). The scale variation changes the ratio by less than ± 0.001 and is not displayed in the table.

	Scenario 1	Scenario 2	Scenario 3
σ_{QCDW} [pb]	$643.22^{+81.23}_{-77.71}$	$624.25^{+80.98}_{-76.19}$	$619.56^{+81.05}_{-75.72}$
σ_{2HDM} [pb]	$13.59^{+1.85}_{-1.64}$	$7.4^{+0.77}_{-0.78}$	$7.21^{+0.81}_{-0.77}$
$\sigma_{\text{2HDM}}/\sigma_{\text{QCDW}}$	0.021	0.012	0.012

We investigate the sensitivity of such an analysis (Fig. 13) by calculating the number of heavy Higgs signal and background events for the dileptonic $t\bar{t}$ final states ($l = e, \mu$)

$$N_{s,b}^{ll} = \mathcal{L} \sigma_{s,b} \text{Br}(t\bar{t} \rightarrow 2l) \epsilon_{ll} \quad (72)$$

and for the lepton plus jets final states ($l = e, \mu$)

$$N_{s,b}^{lj} = \mathcal{L} \sigma_{s,b} \text{Br}(t\bar{t} \rightarrow l + \text{jets}) \epsilon_{lj} \quad (73)$$

assuming the branching ratios

$$\text{Br}(t\bar{t} \rightarrow 2l) = \frac{4}{81}, \quad \text{Br}(t\bar{t} \rightarrow l + \text{jets}) = \frac{24}{81}, \quad (74)$$

an integrated luminosity of $\mathcal{L} = 100 \text{ fb}^{-1}$, and selection efficiencies [78, 79] $\epsilon_{ll} = 0.22$ and $\epsilon_{lj} = 0.12$. We assume that the observed number of events N_{obs} is given by $N_{\text{obs}} = N_s + N_b$,

where N_b is the number of background events without the heavy Higgs bosons and N_{obs} is the total number of events including those from resonant ϕ_2, ϕ_3 production including the Higgs-QCD interference. These events are calculated for $M_{\tilde{t}\tilde{t}}$ windows of different width (20, 80 and 140 GeV). We consider for the lower boundary of the $M_{\tilde{t}\tilde{t}}$ windows the range 340–800 GeV in steps of 20 GeV. We determine from the number of signal and background events the significance Z_{PL} [80, 81] based on the profile likelihood method for each $M_{\tilde{t}\tilde{t}}$ window. In the calculation of Z_{PL} we include an uncertainty on the background of 1% (upper pane in Fig. 13) and⁵ 5% (lower pane in Fig. 13), respectively. Only the significance of the dileptonic channel Z_{PL}^{ll} is shown in Fig. 13. The results for the significance of the lepton plus jets channel Z_{PL}^{lj} are very similar. Figure 13 shows that the significance increases if the $M_{\tilde{t}\tilde{t}}$ window becomes narrower. In wider $M_{\tilde{t}\tilde{t}}$ windows peak values for the signal-to-background ratio are averaged out whereas for smaller windows peaks in the signal-to-background ratio show up as peaks in the significance. Because the experimental resolution is limited we show in Fig. 13 also results for realistic $M_{\tilde{t}\tilde{t}}$ window widths of 80 GeV and 140 GeV. Comparing the upper and lower plot in Fig. 13 where we have assumed a 1% and 5% background uncertainty, respectively, we observe that increasing the assumed uncertainty by a factor of 5 leads to a reduction of the significance by a factor of 1/5. This is due to

$$\lim_{N_b \rightarrow \infty} Z_{\text{PL}} = \frac{\sqrt{2(\eta - \ln(1 + \eta))}}{\varepsilon}, \quad (75)$$

where η is the signal-to-background ratio and ε is the relative background uncertainty. This emphasizes the importance of reducing background uncertainties.

In Table 8 we show numerical values of the significances Z_{PL}^{ll} and Z_{PL}^{lj} for all three scenarios using $M_{\tilde{t}\tilde{t}}$ windows of 80 GeV width. The values for $Z_{\text{PL},1\%}^{ll}$ and $Z_{\text{PL},5\%}^{ll}$ for scenario 1 can be directly compared to Fig. 13. The lepton plus jets decay channel has considerably higher event numbers than the dileptonic channel because of the higher branching ratio. However, the significance in both channels is almost the same. This is because we fixed the relative background uncertainty and the signal-to-background ratio is independent of the channel. A further increase of the luminosity would thus only marginally increase the significance, given a constant relative uncertainty of the background [see also Eq. (75)]. We have also calculated the significances based on the p -value of the Poisson distribution from the number of observed events N_{obs} and background events N_b ignoring the uncertainty. The resulting values for these significances become unreasonably high and cannot be trusted.

In Fig. 14 we show for the $M_{\tilde{t}\tilde{t}}$ distribution a comparison of 8 TeV data from the CMS experiment [27] with theoretical predictions obtained within scenario 1. One can see that the current experimental and theoretical accuracy is insufficient to establish or exclude scenario 1.

⁵ According to Table 7 the theory uncertainty of the background calculated at NLO is about 13%. The uncertainties of the NLO background cross sections within the $M_{\tilde{t}\tilde{t}}$ windows used in Fig. 13 are roughly the same. These uncertainties would reduce the significance Z_{PL} to a value below 1. However, we expect that the uncertainty of 13% can be reduced by using higher order QCD predictions of the background, in particular the next-to-next-to-leading order QCD corrections to $\tilde{t}\tilde{t}$ production [82, 83] and by using a sideband analysis to determine the background in the signal region.

Table 8: Number of events (N) and significance (Z) for the dileptonic (superscript ll) and lepton plus jets (superscript lj) channels ($l = e, \mu$) at $\sqrt{s} = 13$ TeV assuming an integrated luminosity of $\mathcal{L} = 100 \text{ fb}^{-1}$ at the LHC.

	scenario 1		scenario 2		scenario 3	
$M_{t\bar{t}}$ cut (GeV)	460–540	540–620	480–560	560–640	420–500	500–580
N_b^{ll}	153517	90050	130718	76566	190486	113261
N_{obs}^{ll}	160536	88250	135112	76357	196907	111712
$Z_{\text{PL},1\%}^{ll}$	4.4	1.9	3.2	0.3	3.3	1.3
$Z_{\text{PL},5\%}^{ll}$	0.9	0.4	0.7	0.1	0.7	0.3
N_b^{lj}	502422	294711	427805	250582	623410	370675
N_{obs}^{lj}	525393	288819	442186	249897	644423	365603
$Z_{\text{PL},1\%}^{lj}$	4.5	2	3.3	0.3	3.3	1.4
$Z_{\text{PL},5\%}^{lj}$	0.9	0.4	0.7	0.1	0.7	0.3

Table 9: $M_{t\bar{t}}$ windows used in the computation of the y_t and $\cos\theta_{CS}$ distributions.

	Lower $M_{t\bar{t}}$ window	Upper $M_{t\bar{t}}$ window
Scenario 1	$390 \text{ GeV} \leq M_{t\bar{t}} \leq 540 \text{ GeV}$	$540 \text{ GeV} \leq M_{t\bar{t}} \leq 690 \text{ GeV}$
Scenario 2	$410 \text{ GeV} \leq M_{t\bar{t}} \leq 560 \text{ GeV}$	$560 \text{ GeV} \leq M_{t\bar{t}} \leq 710 \text{ GeV}$
Scenario 3	$350 \text{ GeV} \leq M_{t\bar{t}} \leq 500 \text{ GeV}$	$500 \text{ GeV} \leq M_{t\bar{t}} \leq 650 \text{ GeV}$

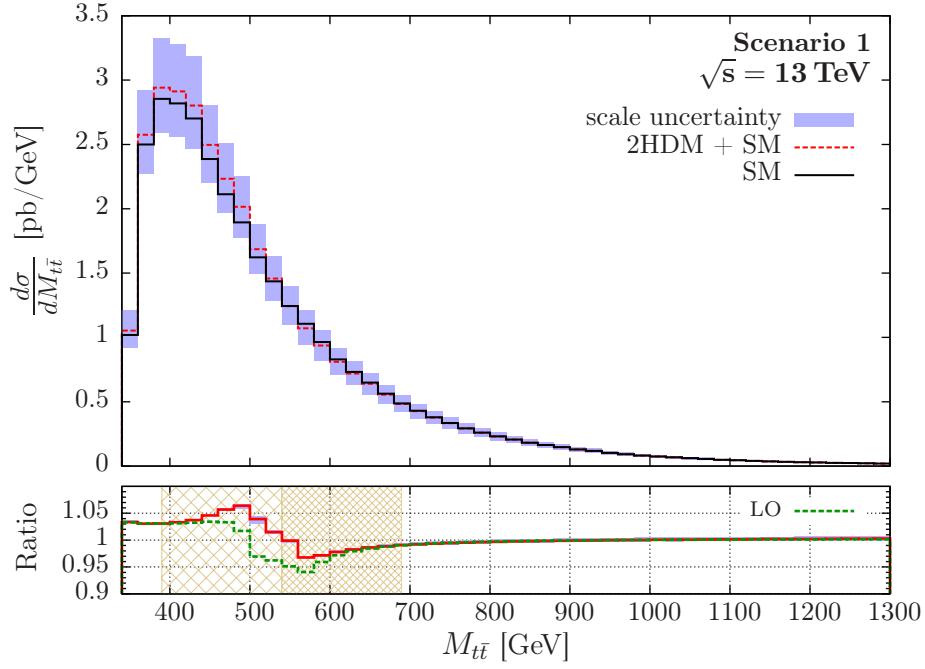


Figure 10: Invariant mass distribution $M_{t\bar{t}}$ of $t\bar{t}$ for scenario 1 at NLO. The upper pane shows the SM contribution (solid black) which includes NLO QCD and weak corrections. The dashed red line shows the sum of SM and 2HDM contributions at NLO QCD. The shaded blue area represents the scale uncertainty when varying $\mu_R = \mu_F = \mu_0$ by a factor of 2 or 1/2, respectively, in the combined SM + 2HDM result. The lower pane shows the sum of SM and 2HDM contributions normalized to the SM contribution at NLO (solid red) and LO (dashed green). The scale uncertainty (shaded blue) of the ratio is very small and is invisible for most of the bins in this plot. The hatched regions in the lower pane indicate the range of the $M_{t\bar{t}}$ cuts.

Furthermore, the limits on the cross section for a spin-zero resonance stated in Ref. [27] were derived without taking interference effects between signal and background into account. There is a more recent ATLAS analysis on resonances in the $M_{t\bar{t}}$ distribution, Ref. [28], but it is also not sensitive enough to establish or exclude our scenarios.

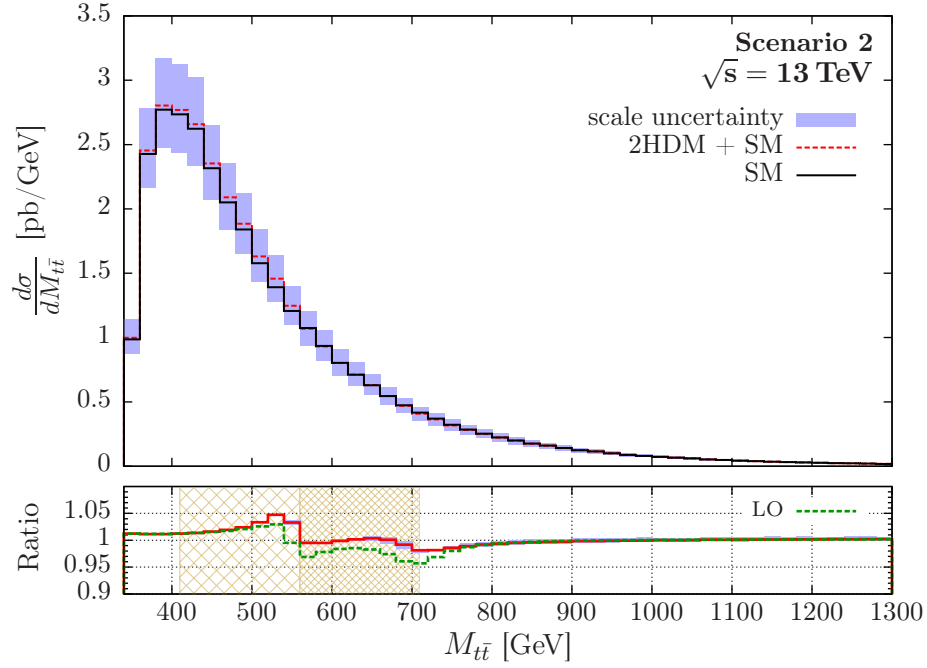


Figure 11: Same as Fig. 10, but for scenario 2.

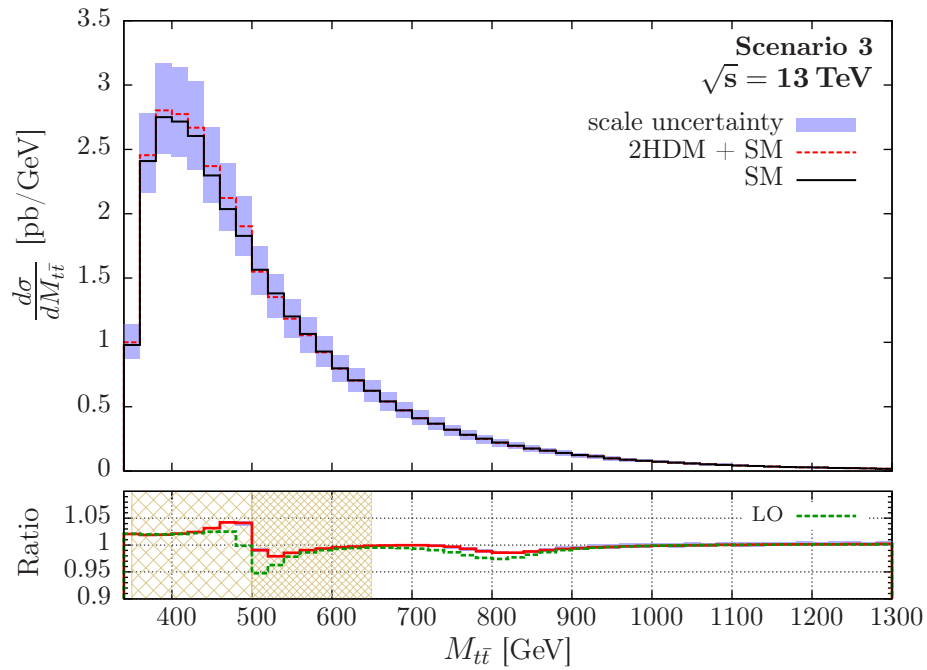


Figure 12: Same as Fig. 10, but for scenario 3.

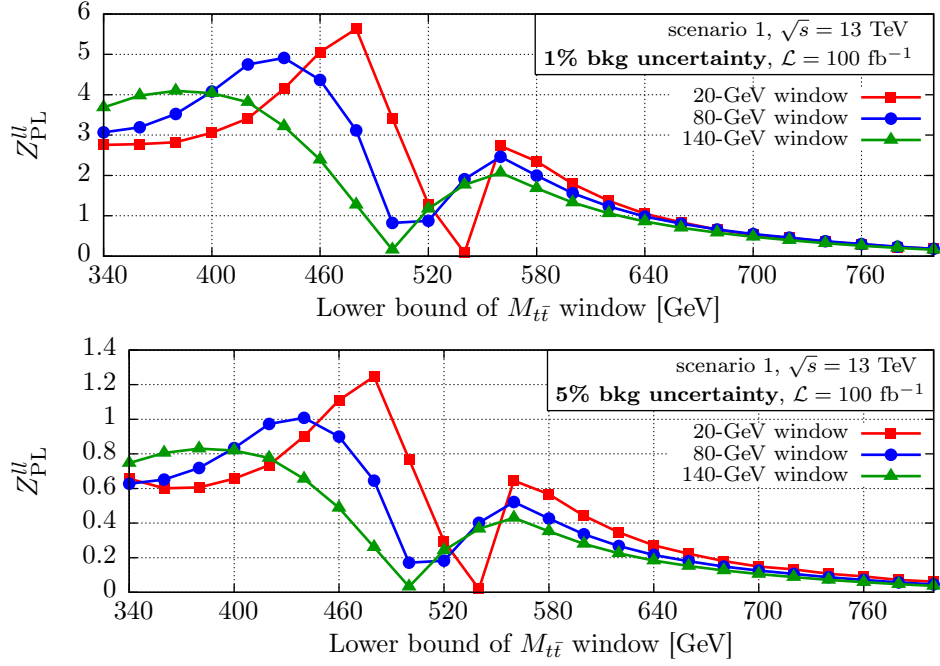


Figure 13: Significance Z_{PL}^l for different cuts on $M_{t\bar{t}}$. The solid red (dashed blue, dotted green) curve shows the behavior for $M_{t\bar{t}}$ windows of 20 GeV (80 GeV, 140 GeV) width. On the abscissa the lower boundaries of the $M_{t\bar{t}}$ windows are given. The upper (lower) pane shows the results for Z_{PL}^l where a 1% (5%) uncertainty on the background is assumed.

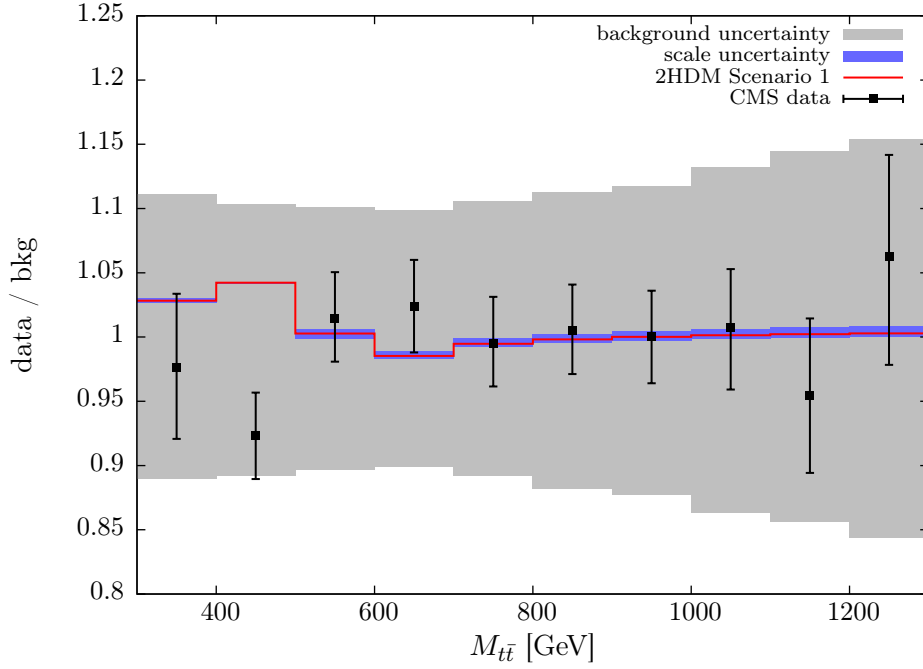


Figure 14: $M_{t\bar{t}}$ distribution for $pp \rightarrow t\bar{t}X$ at the LHC (8 TeV). The black data points were extracted from Fig. 4(b) of Ref. [27] using the tool EasyNData [84]. For error bars not visible in the original plot the radius of the black circle representing the respective data point is used as the error bar length. The shaded grey area was also extracted from Fig. 4(b) of Ref. [27]. It displays the theoretical uncertainty of the background Monte Carlo prediction. The solid red curve in this plot shows our result for scenario 1 including NLO QCD corrections. The shaded blue area represents the scale uncertainty due to the variation of $\mu_R = \mu_F = \mu_0$ by a factor of 2 or 1/2, respectively.

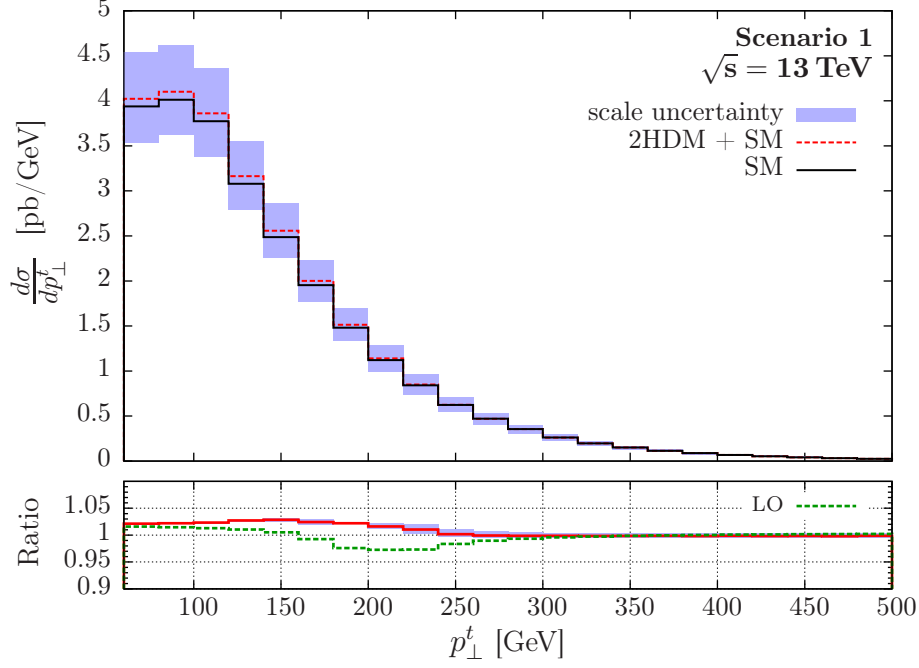


Figure 15: Transverse momentum distribution of the top quark p_{\perp}^t in scenario 1 of the 2HDM at NLO. The upper pane shows the SM contribution (solid black) which includes NLO QCD and weak corrections. The dashed red line displays the sum of the SM contribution and 2HDM contribution at NLO QCD. The shaded blue area represents the scale uncertainty when varying $\mu_R = \mu_F = \mu_0$ by a factor of 2 or 1/2, respectively, in the combined SM + 2HDM result. The plot in the lower pane shows the sum of SM and 2HDM contributions normalized to the SM contribution at NLO (solid red) and LO (dashed green). The scale uncertainty (shaded blue) of the ratio is very small and is invisible for most of the bins in this plot.

The distributions of the top-quark transverse momentum p_{\perp}^t are displayed in Figs. 15–17 for scenarios 1–3, respectively. These distributions are computed without $M_{t\bar{t}}$ cuts. A cut on the $M_{t\bar{t}}$ value in the p_{\perp}^t distribution restricts the Born contribution and the virtual corrections to values $p_{\perp}^t \leq \sqrt{(M_{t\bar{t}}^{\text{cut}})^2/4 - m_t}$. As a consequence the results are only leading order in the strong coupling constant for $p_{\perp}^t > \sqrt{(M_{t\bar{t}}^{\text{cut}})^2/4 - m_t}$. As in the case of the $M_{t\bar{t}}$ distribution the QCD corrections to the 2HDM scenarios are mainly positive such that the ratios of the p_{\perp}^t distributions in all three scenarios stay above one. However, the deviations from one are small. As a remnant of the resonance structure an enhancement around $p_{\perp}^t \approx m_i/2$ can be observed.

In the following we present, for the LHC (13 TeV), a number of distributions for $t\bar{t}$ events obeying the $M_{t\bar{t}}$ cuts given in Table 9. The top-quark rapidity distributions in the laboratory frame, y_t , are displayed in Figs. 18–20 for scenarios 1–3, respectively. As expected the y_t distributions—and the rapidity distributions of the \bar{t} quarks, which are not shown—are (within small statistical fluctuations) symmetric around $y_t = 0$. The impact of the heavy Higgs bosons

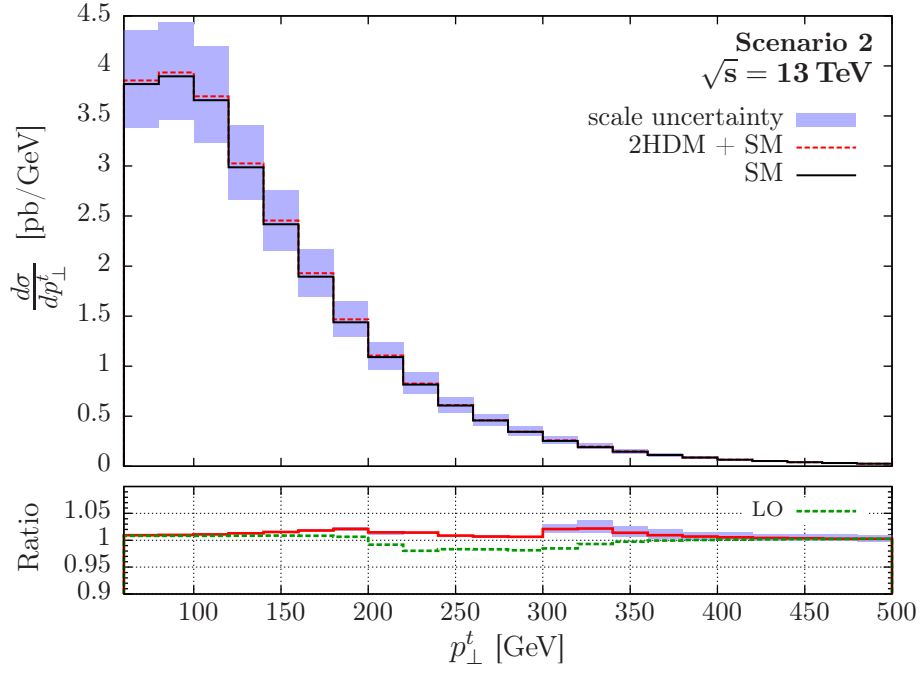


Figure 16: Same as Fig. 15, but for scenario 2.

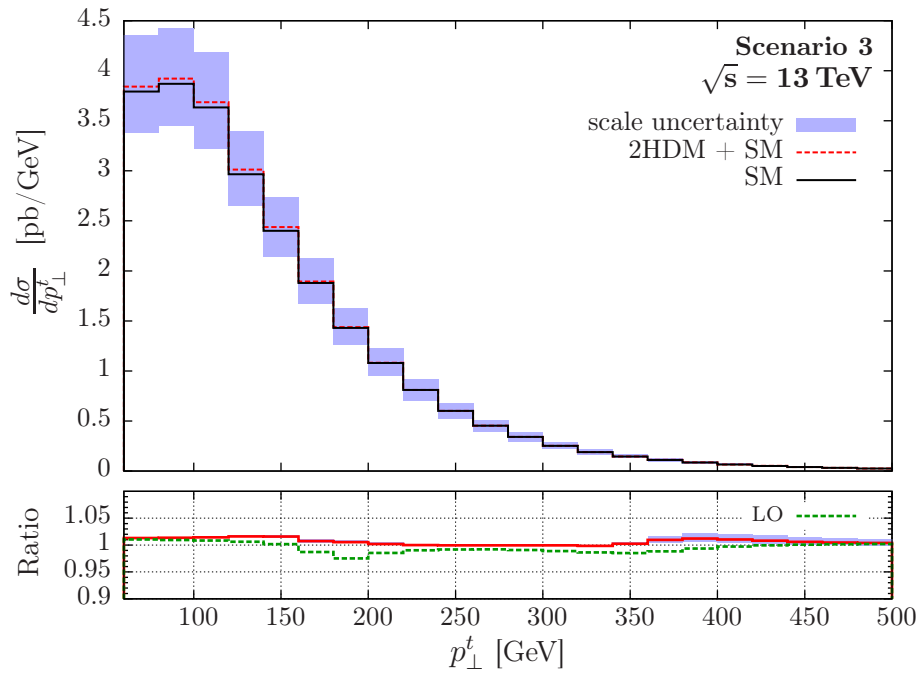


Figure 17: Same as Fig. 15, but for scenario 3.

is rather small, it is maximally $\sim 5\%$ in the central region for scenario 1 in the low $M_{t\bar{t}}$ window. Top-quark pair production by $q\bar{q}$ annihilation and (anti)quark gluon fusion at NLO QCD induces a small asymmetry in the distribution of the moduli difference $\Delta|y| = |y_t| - |y_{\bar{t}}|$. The inclusive $t\bar{t}$ charge asymmetry $A_C = [N(\Delta|y| > 0) - N(\Delta|y| < 0)]/N_{\text{tot}}$ at 13 TeV (integrated over $M_{t\bar{t}}$) is $A_C = 0.75(5) \times 10^{-2}$ at NLO QCD including electroweak corrections. The heavy Higgs boson contributions, which are symmetric with respect to the interchange of t and \bar{t} , do not change this result.

The distributions of the cosine of the Collins-Soper angle [30] $\cos\theta_{CS}$ are shown in Figs. 21–23 for scenarios 1–3, respectively. We recall that θ_{CS} is similar to the angle between the top quark and the direction of one of the beams in the $t\bar{t}$ zero-momentum frame (ZMF)—in fact, at leading order they are identical—, but θ_{CS} is less affected by initial state radiation. Let us denote the momenta of the two proton beams in the $t\bar{t}$ ZMF by p_1 and p_2 . If the transverse momentum of the $t\bar{t}$ pair is nonzero the three-momenta \mathbf{p}_1 and \mathbf{p}_2 are not collinear, and θ_{CS} is defined to be the angle between the top-quark direction in the $t\bar{t}$ ZMF and the bisecting line between \mathbf{p}_1 and $-\mathbf{p}_2$. For the production of a spin-zero resonance and its decay to $t\bar{t}$ the $\cos\theta_{CS}$ distribution is flat at LO. For the background at LO QCD, one gets for $q\bar{q} \rightarrow t\bar{t}$ a distribution proportional to $\hat{s}(1 + \cos^2\theta_{CS}) + 4m_t^2(1 - \cos^2\theta_{CS})$. For $gg \rightarrow t\bar{t}$, where all partial waves are present, the $\cos\theta_{CS}$ distribution is more complicated, but is also minimal in the central region and maximal in the forward and backward region. The background distributions computed at NLO QCD including weak corrections, which are displayed in Figs. 21–23, corroborate this behavior. Adding the contributions of the heavy Higgs bosons and the interference with the background changes the shape of the $\cos\theta_{CS}$ distributions only moderately. The effect is largest in the low $M_{t\bar{t}}$ window of scenario 1, where the distribution changes by $\sim 6\%$ in the central region.

Finally, we have also calculated the above distributions for 14 TeV. We do not display them here because these results are similar to those for 13 TeV and do not bear significant new insights.

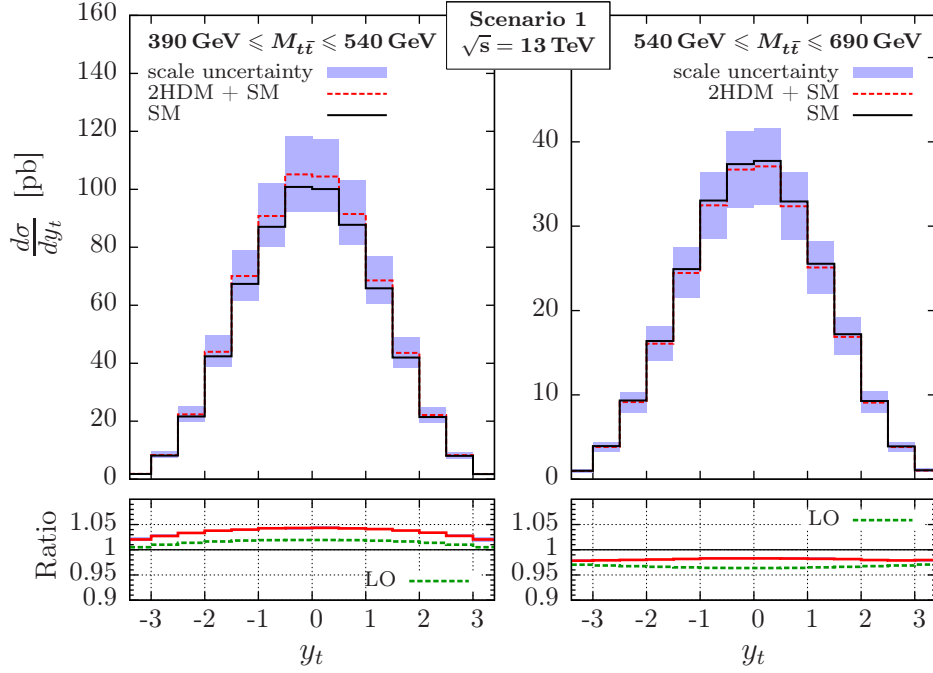


Figure 18: Top-quark rapidity distribution y_t for scenario 1 of the 2HDM at NLO. The plots in the upper panes show the SM contribution (solid black) which includes NLO QCD and weak corrections. The dashed red line shows the sum of the SM contribution and 2HDM contribution at NLO QCD. The shaded blue area represents the scale uncertainty when varying $\mu_R = \mu_F = \mu_0$ by a factor of 2 or 1/2, respectively, in the combined SM + 2HDM result. The plots in the lower panes show the sum of SM and 2HDM contributions normalized to the SM contribution at NLO (solid red) and LO (dashed green). The scale uncertainties (shaded blue) of the ratios are very small and are invisible in these plots. The plots on the left- and right-hand side correspond to different $M_{t\bar{t}}$ windows.

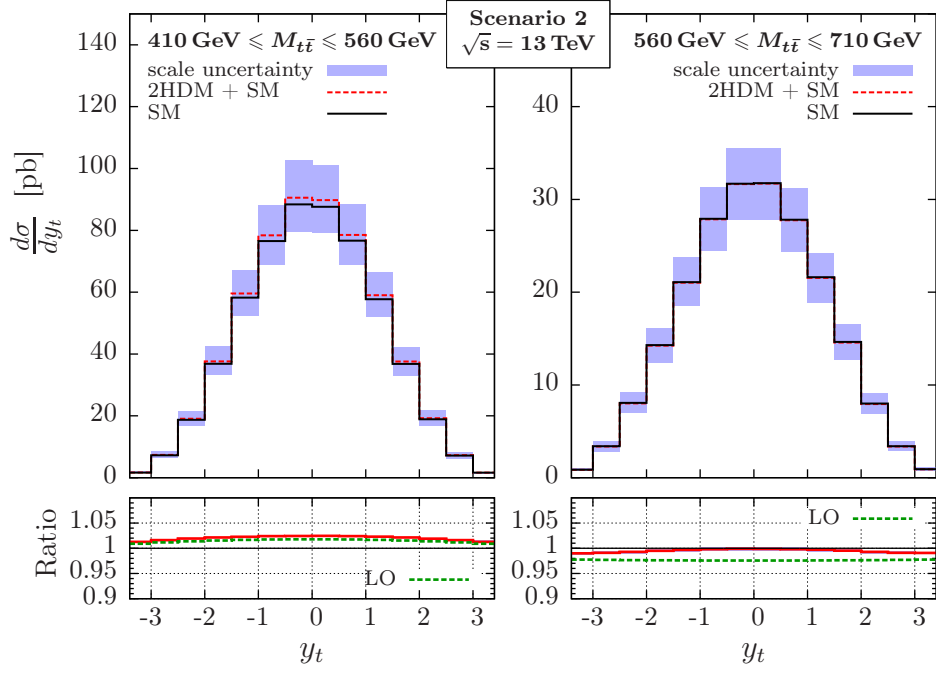


Figure 19: Same as Fig. 18, but for scenario 2 and different $M_{t\bar{t}}$ windows.

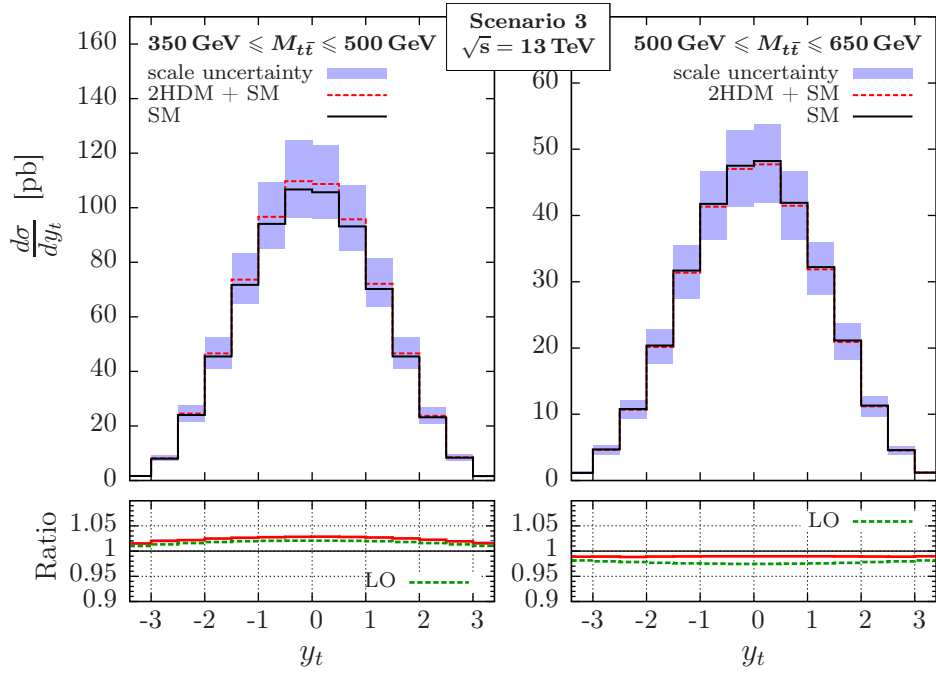


Figure 20: Same as Fig. 18, but for scenario 3 and different $M_{t\bar{t}}$ windows.

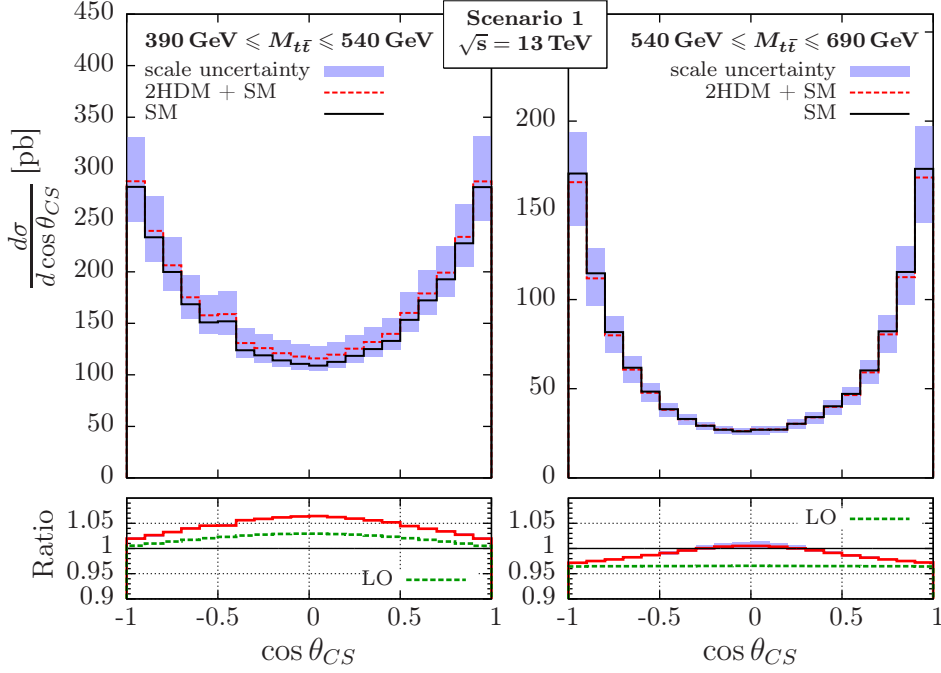


Figure 21: Distribution of the cosine of the Collins-Soper angle, $\cos\theta_{CS}$, for the top quark in scenario 1 of the 2HDM at NLO. The plots in the upper panes show the SM contribution (solid black) which includes NLO QCD and weak corrections. The dashed red line displays the sum of the SM contribution and 2HDM contribution at NLO QCD. The shaded blue area represents the scale uncertainty when varying $\mu_R = \mu_F = \mu_0$ by a factor of 2 or 1/2, respectively, in the combined SM + 2HDM result. The plots in the lower panes show the sum of SM and 2HDM contributions normalized to the SM contribution at NLO (solid red) and LO (dashed green). The scale uncertainties (shaded blue) of the ratios are very small and are invisible for most of the bins in these plots. The plots on the left- and right-hand side correspond to different $M_{t\bar{t}}$ windows.

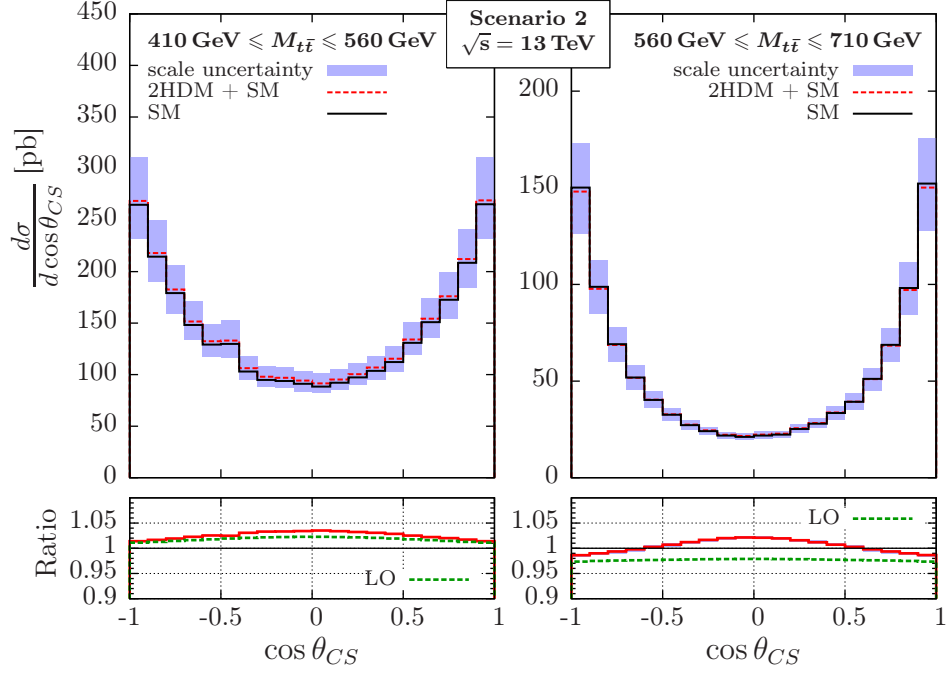


Figure 22: Same as Fig. 21, but for scenario 2 and different $M_{t\bar{t}}$ windows.

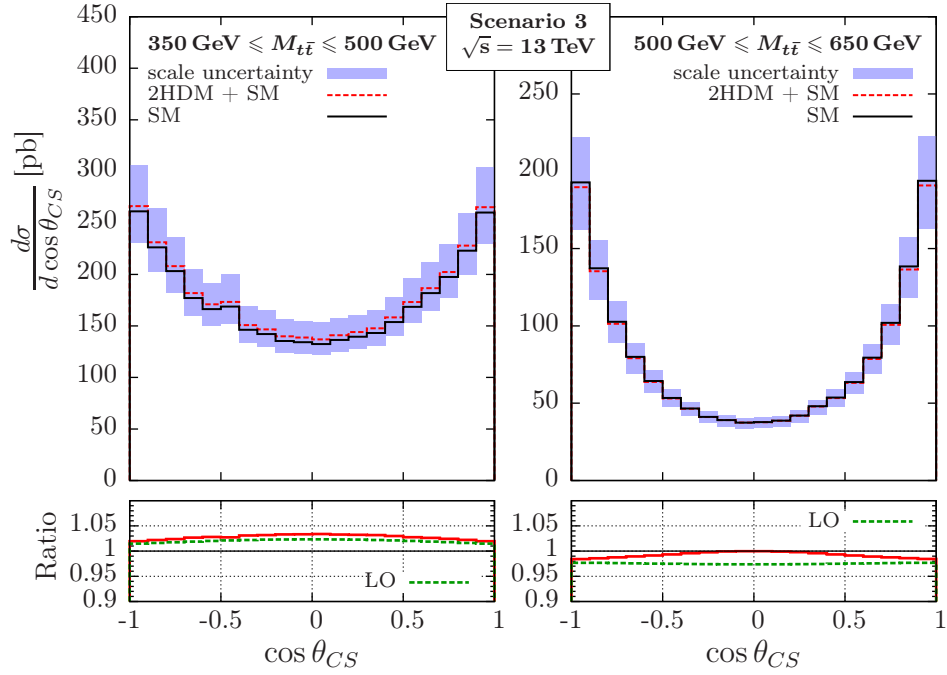


Figure 23: Same as Fig. 21, but for scenario 3 and different $M_{t\bar{t}}$ windows.

6. Summary and conclusions

This paper is based on the hypothesis that in addition to the 125 GeV Higgs boson additional heavy neutral Higgs bosons with unsuppressed Yukawa couplings to top quarks exist, which can be resonantly produced at the LHC in the $t\bar{t}$ channel. The analysis of $t\bar{t}$ data at the LHC, which so far has been rather rudimentary with regard to this possibility, requires precise theoretical predictions. We have therefore investigated effects of heavy, neutral Higgs boson resonances in $t\bar{t}$ production at the LHC at next-to-leading order in the strong coupling. A new ingredient of our analysis is the incorporation of the interferences of the heavy Higgs production amplitudes with the respective nonresonant QCD $t\bar{t}$ amplitudes at NLO QCD. The NLO corrections to heavy Higgs boson production and the Higgs-QCD interference were computed in the large m_t limit with an effective K-factor rescaling. The nonresonant $t\bar{t}$ background was incorporated at NLO QCD including weak-interaction corrections.

Our NLO QCD computation of heavy Higgs production and decay into $t\bar{t}$ and the interference with the nonresonant $t\bar{t}$ amplitude is in principle rather model independent. However, essential ingredients in our analysis are the total decay widths of the heavy Higgs bosons, which must be computed in a concrete model in order to maintain the unitarity of the S -matrix. To be specific, we used the type-II two-Higgs-doublet model where three neutral Higgs bosons appear in the physical particle spectrum. We investigated three phenomenologically viable parameter scenarios in more detail, where one of these particles is identified with the 125 GeV Higgs boson. We considered parameter sets of this model where this boson has SM-like couplings to the quarks, leptons, and weak gauge bosons. The masses of the other two neutral Higgs bosons were assumed to lie above the $t\bar{t}$ threshold, with top-quark Yukawa couplings that are slightly larger than the SM top-quark Yukawa coupling.

For these three parameter sets we investigated heavy Higgs boson production and decay to $t\bar{t}$ at the LHC operating at 13 TeV. We computed the inclusive $t\bar{t}$ cross section and the $t\bar{t}$ invariant mass distribution with and without the two heavy Higgs resonances. Assuming an integrated luminosity of 100 fb^{-1} , we estimated, for appropriately chosen $M_{t\bar{t}}$ intervals and our three parameter scenarios, the significances for detecting a heavy Higgs signal in the $t\bar{t}$ dileptonic and lepton plus jets decay channels. In addition we computed the top-quark transverse momentum distribution and, for selected $M_{t\bar{t}}$ windows, the top-quark rapidity distribution and that of the cosine of the Collins-Soper angle. We showed also that the so-far negative results by the CMS and ATLAS experiment on searches for heavy spin-zero resonances in the $t\bar{t}$ channel at the LHC (8 TeV) do not exclude our parameter scenarios.

Because the masses of the heavy Higgs resonances are not known, we propose to scan the $t\bar{t}$ invariant mass distribution with a sliding $M_{t\bar{t}}$ window of width $\Delta M_{t\bar{t}} \sim 80 \text{ GeV}$. Mass bins of this size are experimentally feasible, at least for $M_{t\bar{t}} \lesssim 1 \text{ TeV}$. Our analysis of Sec. 5 shows that, for our parameter scenarios, the significances for detecting a heavy Higgs resonance exceed 3σ only if the uncertainties involved in measuring $M_{t\bar{t}}$ windows and modeling the nonresonant $t\bar{t}$ background can be pushed down to a level of $\sim 1\%$. Such a precision is unrealistic at present, but since both theoretical and experimental uncertainties in measuring the (binned)

$t\bar{t}$ cross section have been significantly reduced in recent years, one may be optimistic and expect further improvements also in the future. Full multivariate experimental analyses, which increase the sensitivity, would also use information from other distributions, including those considered in Sec. 5. A further set of observables, which we plan to investigate in future work, includes $t\bar{t}$ spin correlation and t, \bar{t} polarization observables. Such observables show, in selected $M_{t\bar{t}}$ windows, also some sensitivity to heavy Higgs resonances and potentially allow one to discriminate between a scalar, a pseudoscalar, and a CP mixture.

Acknowledgments

W.B. thanks A. Brandenburg for a discussion. This work was supported in part by Deutsche Forschungsgemeinschaft (DFG) Grant No. SFB-TR09. P. G. was supported by DFG through Graduiertenkolleg Grant No. GRK 1504 and C. M. through DFG Graduiertenkolleg Grant No. GRK 1675. The work of Z.G. S. was supported by National Natural Science Foundation of China and by Natural Science Foundation of Shandong Province.

A. Description of Higgs resonances

The unstable particles which are involved in the reactions considered in this paper are the weak gauge bosons, and the three neutral Higgs bosons of the 2HDM extension of the SM. The charged Higgs boson does not play any role here—see the 2HDM scenarios considered in Sec. 3. The top quark, too, is of course unstable, but in this paper we consider reactions at the level of t and \bar{t} final states. The following discussion applies also if top-quark decays are incorporated into the analysis. While we take higher order QCD corrections to the parton reactions $ab \rightarrow t\bar{t} + X$ into account we emphasize that we incorporate the weak gauge boson and Yukawa interactions only to leading order. This is important to keep in mind in the following discussion.

As argued above, the top quark can be treated in the narrow width approximation. The Z boson appears in $t\bar{t} + X$ production as s -channel resonance only far off shell, $Z^* \rightarrow t\bar{t} + X$. Hence its width can be safely neglected. The same statement applies to the light Higgs boson ϕ_1 with⁶ $m_1 = 125$ GeV. The W^\pm boson is resonantly produced in t and \bar{t} decay, respectively. As we work to lowest order in the weak gauge couplings this can be incorporated by using the width Γ_W in the W -boson propagator.

In the resonant production of the heavy Higgs bosons, $ab \rightarrow \phi_{2,3} \rightarrow t\bar{t} + X$, the finite width effects must be accounted for. The adequate method which respects gauge invariance also with respect to higher order electroweak corrections is the so-called complex mass scheme [55–57]. Let us illustrate this method for the case at hand, using only one ϕ . We consider the amplitude for the process $ab \rightarrow \phi \rightarrow t\bar{t} + X$, including only factorizable QCD corrections. The

⁶The total width of ϕ_1 is SM-like, i.e. very small in the 2HDM scenarios considered below, $\Gamma_1 \sim 4$ MeV.

nonfactorizable QCD corrections are analyzed in Sec. 4.2 and Appendix B. In the complex mass scheme the amplitude is of the form

$$\mathcal{M}_{i \rightarrow f} = S_{ij}(k^2, \dots) iP(k^2) S_f(k^2, \dots) + \mathcal{N}, \quad P(k^2) = \frac{1}{k^2 - \mu_\phi^2}, \quad (76)$$

where the complex mass parameter μ_ϕ^2 is the pole of the full ϕ propagator, i.e., the point in the complex s plane where the renormalized Higgs boson self energy $\Pi(s)$ vanishes:

$$\Pi(\mu_\phi^2) = 0. \quad (77)$$

The symbol \mathcal{N} in Eq. (76) denotes the nonresonant contribution to the scattering matrix element. The complex mass parameter must be used wherever the ϕ mass squared occurs in the scattering amplitude. However, as we compute (76) only to lowest order in the weak and Yukawa interactions, μ_ϕ^2 does not appear in the loops contributing to S_{ij} and S_f , but only in $P(s)$. We parametrize

$$\mu_\phi^2 = m^2 - im\Gamma. \quad (78)$$

The meaning of m and Γ is as follows. The relation between the renormalized and bare Higgs boson self energy is, to one-loop order in the electroweak and Yukawa couplings,

$$\Pi(k^2) = \Pi_0(k^2) - \delta\mu_\phi^2 + (k^2 - \mu_\phi^2)\delta\mathcal{Z}_\phi, \quad (79)$$

where $\mathcal{Z}_\phi = 1 + \delta\mathcal{Z}_\phi$ is the complex Higgs wave-function renormalization constant and $\delta\mu_\phi^2$ is the complex mass counterterm. The relation between the *real* bare Higgs mass squared, m_0^2 , and the complex renormalized mass squared μ_ϕ^2 is

$$m_0^2 = \mu_\phi^2 + \delta\mu_\phi^2. \quad (80)$$

The condition (77) is the complex-mass-scheme generalization of the usual on-shell renormalization condition. Using (79) it implies that

$$\delta\mu_\phi^2 = \Pi_0(\mu_\phi^2). \quad (81)$$

Now we use the parametrization (78) and the relation (80), i.e., $\delta\mu_\phi^2 = m_0^2 - \mu_\phi^2$. Taking the real part of this relation shows that m can be interpreted as the on-shell mass of ϕ . Taking the imaginary part gives the equation

$$m\Gamma = \text{Im}\Pi_0(m^2 - im\Gamma), \quad (82)$$

which in general can be solved iteratively for Γ . Expanding this relation around m , one gets to one-loop order in the electroweak and Yukawa couplings [56]:

$$m\Gamma = \text{Im}\Pi_0(m^2) - m\Gamma \text{Re}\Pi_0'(m^2), \quad (83)$$

where the prime denotes the derivative with respect to k^2 . Again, this equation may be solved iteratively for Γ . Because we work to lowest order in the weak and Yukawa couplings we can neglect the second term in (83). Then Γ is the total ϕ -boson width in the usual on-shell scheme.

In summary we use (76) where μ_ϕ^2 is determined by the on-shell mass and total width of the respective Higgs boson ϕ_2, ϕ_3 .

B. Cancellation of real and virtual nonfactorizable corrections in the soft gluon approximation

As an example for the cancellation of real and virtual nonfactorizable corrections in the SGA we take the amplitude depicted in Fig. 6. The dotted red cut in Fig. 6 corresponds to the interference of two Feynman diagrams contributing to the real corrections and the dashed green cut indicates the interference of the one-loop diagram shown in Fig. 5 with the s -channel QCD Born diagram. We start with the latter interference. In the SGA the loop integral for the amplitude shown in Fig. 5 reduces to the scalar integral

$$\int \frac{d^4\ell}{(2\pi)^4} \frac{\mathcal{N}_{\text{virt}}}{[\ell^2 + i\varepsilon][-2\ell \cdot p_1 + i\varepsilon][-2\ell \cdot (p_1 + p_2) + s - m_\phi^2 + i\varepsilon][-2\ell \cdot k_1 + i\varepsilon]}, \quad (84)$$

where ℓ is the loop momentum which is required to be soft within the SGA. The numerator $\mathcal{N}_{\text{virt}}$ in the SGA is obtained from the exact numerator by setting $\ell = 0$. The momenta of the incoming gluons are denoted p_1 and p_2 , and k_1 is the momentum of the outgoing top quark. In the last three square brackets of the denominator of (84) the ℓ^2 terms are neglected, which is also part of the SGA. The integration over the ℓ^0 component is performed in the complex ℓ^0 plane using the residue theorem. Closing the contour in the lower half of the plane the residue of the pole of the first propagator in Eq. (84) is picked up. The location of the poles of the other propagators is in the upper half of the ℓ^0 plane. Ignoring the numerator the following result is obtained:

$$\begin{aligned} & -i \int \frac{d^3\ell}{(2\pi)^3} \frac{1}{2|\ell|} \frac{1}{[-2|\ell|p_1^0 + 2\ell \cdot \mathbf{p}_1 + i\varepsilon]} \\ & \times \frac{1}{[-2|\ell|(p_1^0 + p_2^0) + 2\ell \cdot (\mathbf{p}_1 + \mathbf{p}_2) + s - m_\phi^2 + i\varepsilon][-2|\ell|k_1^0 + 2\ell \cdot \mathbf{k}_1 + i\varepsilon]} \\ & = i \int \frac{d^3\ell}{(2\pi)^3} \frac{1}{2\ell^0} \frac{1}{[-2\ell \cdot p_1 + i\varepsilon][-2\ell \cdot (p_1 + p_2) + s - m_\phi^2 + i\varepsilon][2\ell \cdot k_1 - i\varepsilon]} \end{aligned} \quad (85)$$

with $|\ell| = \ell^0$. The integration measure $d^3\ell/[(2\pi)^3 2\ell^0]$ is identical to the Lorentz invariant phase-space measure of the gluon. What remains to be done is to show that Eq. (85) including the numerator indeed corresponds to the phase-space integral over the soft gluon in the corresponding real correction contribution. Thus we analyze the interference term indicated in Fig. 6 by the dotted red cut. After applying the SGA this interference leads to the following propagator structure,

$$\frac{1}{[-2q \cdot p_1 + i\varepsilon][-2q \cdot (p_1 + p_2) + s - m_\phi^2 + i\varepsilon][2q \cdot k_1 - i\varepsilon]}, \quad (86)$$

where q is the four-momentum of the (soft) gluon. Taking the phase-space integration over the soft gluon momentum q into account,

$$\int \frac{d^3q}{(2\pi)^3} \frac{1}{2q^0} \frac{1}{[-2q \cdot p_1 + i\varepsilon][-2q \cdot (p_1 + p_2) + s - m_\phi^2 + i\varepsilon][2q \cdot k_1 - i\varepsilon]}, \quad (87)$$

the two expressions Eq. (85) and Eq. (87) are identical up to a factor of i .

So far only the denominators were investigated and the numerators of the amplitudes were ignored. It remains to show that they are identical up to a sign. The real radiation amplitude leads to

$$\begin{aligned} \mathcal{N}_{\text{real}} &= \text{Tr}[(\not{k}_1 + m_t)V_{\phi tt}(\not{k}_2 - m_t)V_{gtt,\alpha_2}^{c_2}(\not{k}_1 + m_t)V_{gtt}^{\rho',c_3}] \\ &\times V_{ggg}^{\mu'\nu'\alpha_2,abc_2}(p_1, p_2, -p_1 - p_2)V_{ggg}^{\mu\alpha_1\rho,ac_1c_3}(p_1, -p_1, 0)V_{gg\phi,\alpha_1}^{\nu,bc_1}(p_2, p_1) \\ &\times \frac{\mathcal{P}_{\mu\mu'}(p_1, p_2)\mathcal{P}_{\nu\nu'}(p_2, p_1)\mathcal{P}_{\rho\rho'}(q, n)}{(p_1 + p_2)^2}, \end{aligned} \quad (88)$$

where

$$V_{\phi tt} = -i\frac{m_t}{v}(a_t - ib_t\gamma_5), \quad (89)$$

$$V_{gtt}^{\mu,a} = -ig_s t^a \gamma^\mu, \quad (90)$$

$$V_{ggg}^{\mu\nu\rho,abc}(p_1, p_2, p_3) = -g_s f^{abc}(g^{\mu\nu}(p_1 - p_2)^\rho + g^{\nu\rho}(p_2 - p_3)^\mu + g^{\rho\mu}(p_3 - p_1)^\nu), \quad (91)$$

$$V_{gg\phi}^{\mu\nu,ab}(p_1, p_2) = -4i\delta^{ab}[f_S^{(0)}(g^{\mu\nu}p_1 \cdot p_2 - p_1^\nu p_2^\mu) - 2f_P^{(0)}\epsilon^{\mu\nu\rho\sigma}p_{1\rho}p_{2\sigma}], \quad (92)$$

and $\mathcal{P}_{\alpha\alpha'}$ is the gluon polarization sum

$$\mathcal{P}_{\alpha\alpha'}(p, n) = -g_{\alpha\alpha'} + \frac{p_\alpha n_{\alpha'} + p_{\alpha'} n_\alpha}{p \cdot n}, \quad n^2 = 0, \quad (93)$$

where n is an arbitrary lightlike vector. Instead of the polarization sum in Eq. (93) we use

$$\mathcal{P}_{\rho\rho'}(q, n) = -g_{\rho\rho'}, \quad (94)$$

because in the present case there are no diagrams where the external soft gluon could be replaced by a ghost. With this relation we obtain:

$$\begin{aligned} \mathcal{N}_{\text{real}} &= -\text{Tr}[(\not{k}_1 + m_t)V_{\phi tt}(\not{k}_2 - m_t)V_{gtt,\alpha_2}^{c_2}(\not{k}_1 + m_t)V_{gtt}^{\alpha_3,c_3}] \\ &\times V_{ggg}^{\mu'\nu'\alpha_2,abc_2}(p_1, p_2, -p_1 - p_2)V_{ggg,\alpha_3}^{\mu\alpha_1ac_1c_3}(p_1, -p_1, 0)V_{gg\phi,\alpha_1}^{\nu,bc_1}(p_2, p_1) \\ &\times \frac{\mathcal{P}_{\mu\mu'}(p_1, p_2)\mathcal{P}_{\nu\nu'}(p_2, p_1)}{(p_1 + p_2)^2}. \end{aligned} \quad (95)$$

The numerator of $\mathcal{N}_{\text{virt}}$ of the virtual correction contribution (84) is computed in straightforward fashion in the SGA. One obtains

$$\mathcal{N}_{\text{virt}} = i\mathcal{N}_{\text{real}}. \quad (96)$$

Therefore

$$\begin{aligned} &i \int \frac{d^3\ell}{(2\pi)^3} \frac{1}{2\ell^0} \frac{\mathcal{N}_{\text{virt}}}{[-2\ell \cdot p_1 + i\epsilon][-2\ell \cdot (p_1 + p_2) + s - m_\phi^2 + i\epsilon][2\ell \cdot k_1 - i\epsilon]} \\ &= - \int \frac{d^3\ell}{(2\pi)^3} \frac{1}{2\ell^0} \frac{\mathcal{N}_{\text{real}}}{[-2\ell \cdot p_1 + i\epsilon][-2\ell \cdot (p_1 + p_2) + s - m_\phi^2 + i\epsilon][2\ell \cdot k_1 - i\epsilon]} \end{aligned} \quad (97)$$

which exactly cancels the contribution from the real correction,

$$\int \frac{d^3q}{(2\pi)^3} \frac{1}{2q^0} \frac{\mathcal{N}_{\text{real}}}{[-2q \cdot p_1 + i\varepsilon][-2q \cdot (p_1 + p_2) + s - m_\phi^2 + i\varepsilon][2q \cdot k_1 - i\varepsilon]}. \quad (98)$$

Note that

$$\delta^{(4)}(p_1 + p_2 - k_1 - k_2 - q) \xrightarrow{\text{SGA}} \delta^{(4)}(p_1 + p_2 - k_1 - k_2) \quad (99)$$

in the phase-space integration of (98). Thus the four-momentum conservation matches the one in the phase-space integration of (97).

References

- [1] ATLAS Collaboration, G. Aad et al., *Observation of a new particle in the search for the Standard Model Higgs boson with the ATLAS detector at the LHC*, Phys. Lett. **B716** (2012) 1–29, arXiv:1207.7214 [hep-ex].
- [2] CMS Collaboration, S. Chatrchyan et al., *Observation of a new boson at a mass of 125 GeV with the CMS experiment at the LHC*, Phys. Lett. **B716** (2012) 30–61, arXiv:1207.7235 [hep-ex].
- [3] CMS Collaboration, V. Khachatryan et al., *Precise determination of the mass of the Higgs boson and tests of compatibility of its couplings with the standard model predictions using proton collisions at 7 and 8 TeV*, Eur. Phys. J. **C75** no. 5, (2015) 212, arXiv:1412.8662 [hep-ex].
- [4] ATLAS Collaboration, G. Aad et al., *Measurements of the Higgs boson production and decay rates and coupling strengths using pp collision data at $\sqrt{s} = 7$ and 8 TeV in the ATLAS experiment*, Eur. Phys. J. **C76** no. 1, (2016) 6, arXiv:1507.04548 [hep-ex].
- [5] A. Djouadi, *The Anatomy of electro-weak symmetry breaking. II. The Higgs bosons in the minimal supersymmetric model*, Phys. Rept. **459** (2008) 1–241, arXiv:hep-ph/0503173 [hep-ph].
- [6] G. C. Branco, P. M. Ferreira, L. Lavoura, M. N. Rebelo, M. Sher, and J. P. Silva, *Theory and phenomenology of two-Higgs-doublet models*, Phys. Rept. **516** (2012) 1–102, arXiv:1106.0034 [hep-ph].
- [7] ATLAS Collaboration, *Measurements of the properties of the Higgs-like boson in the four lepton decay channel with the ATLAS detector using 25 fb⁻¹ of proton-proton collision data, ATLAS-CONF-2013-013*,.
- [8] CMS Collaboration, V. Khachatryan et al., *Search for a pseudoscalar boson decaying into a Z boson and the 125 GeV Higgs boson in $\ell^+ \ell^- b\bar{b}$ final states*, Phys. Lett. **B748** (2015) 221–243, arXiv:1504.04710 [hep-ex].

- [9] ATLAS Collaboration, G. Aad et al., *Search For Higgs Boson Pair Production in the $\gamma b\bar{b}$ Final State using pp Collision Data at $\sqrt{s} = 8$ TeV from the ATLAS Detector*, Phys. Rev. Lett. **114** no. 8, (2015) 081802, arXiv:1406.5053 [hep-ex].
- [10] ATLAS Collaboration, G. Aad et al., *Search for a CP-odd Higgs boson decaying to Zh in pp collisions at $\sqrt{s} = 8$ TeV with the ATLAS detector*, Phys. Lett. **B744** (2015) 163–183, arXiv:1502.04478 [hep-ex].
- [11] CMS Collaboration, V. Khachatryan et al., *Search for a Higgs Boson in the Mass Range from 145 to 1000 GeV Decaying to a Pair of W or Z Bosons*, JHEP **10** (2015) 144, arXiv:1504.00936 [hep-ex].
- [12] ATLAS, CMS Collaboration, Y. Nagai, *Higgs Search in $b\bar{b}$ Signatures at ATLAS and CMS*, PoS **Beauty2013** (2013) 001, arXiv:1306.1784 [hep-ex].
- [13] CMS Collaboration, V. Khachatryan et al., *Search for resonant pair production of Higgs bosons decaying to two bottom quark antiquark pairs in protonproton collisions at 8 TeV*, Phys. Lett. **B749** (2015) 560–582, arXiv:1503.04114 [hep-ex].
- [14] CMS Collaboration, V. Khachatryan et al., *Search for neutral MSSM Higgs bosons decaying to a pair of tau leptons in pp collisions*, JHEP **10** (2014) 160, arXiv:1408.3316 [hep-ex].
- [15] ATLAS Collaboration, G. Aad et al., *Search for neutral Higgs bosons of the minimal supersymmetric standard model in pp collisions at $\sqrt{s} = 8$ TeV with the ATLAS detector*, JHEP **11** (2014) 056, arXiv:1409.6064 [hep-ex].
- [16] K. J. F. Gaemers and F. Hoogeveen, *Higgs Production and Decay Into Heavy Flavors With the Gluon Fusion Mechanism*, Phys. Lett. **B146** (1984) 347.
- [17] D. Dicus, A. Stange, and S. Willenbrock, *Higgs decay to top quarks at hadron colliders*, Phys. Lett. **B333** (1994) 126–131, arXiv:hep-ph/9404359 [hep-ph].
- [18] W. Bernreuther and A. Brandenburg, *Tracing CP violation in the production of top quark pairs by multiple TeV proton proton collisions*, Phys. Rev. **D49** (1994) 4481–4492, arXiv:hep-ph/9312210 [hep-ph].
- [19] W. Bernreuther, M. Flesch, and P. Haberl, *Signatures of Higgs bosons in the top quark decay channel at hadron colliders*, Phys. Rev. **D58** (1998) 114031, arXiv:hep-ph/9709284 [hep-ph].
- [20] W. Bernreuther, A. Brandenburg, and M. Flesch, *Effects of Higgs sector CP violation in top quark pair production at the LHC*, arXiv:hep-ph/9812387 [hep-ph].
- [21] V. Barger, T. Han, and D. G. E. Walker, *Top Quark Pairs at High Invariant Mass: A Model-Independent Discriminator of New Physics at the LHC*, Phys. Rev. Lett. **100** (2008) 031801, arXiv:hep-ph/0612016 [hep-ph].
- [22] R. Frederix and F. Maltoni, *Top pair invariant mass distribution: A Window on new*

- physics*, JHEP **01** (2009) 047, arXiv:0712.2355 [hep-ph].
- [23] V. Barger, W.-Y. Keung, and B. Yencho, *Azimuthal Correlations in Top Pair Decays and The Effects of New Heavy Scalars*, Phys. Rev. **D85** (2012) 034016, arXiv:1112.5173 [hep-ph].
- [24] N. Craig, F. D’Eramo, P. Draper, S. Thomas, and H. Zhang, *The Hunt for the Rest of the Higgs Bosons*, JHEP **06** (2015) 137, arXiv:1504.04630 [hep-ph].
- [25] S. Jung, J. Song, and Y. W. Yoon, *Dip or nothingness of a Higgs resonance from the interference with a complex phase*, Phys. Rev. **D92** no. 5, (2015) 055009, arXiv:1505.00291 [hep-ph].
- [26] B. Bhattacharjee, A. Chakraborty, and A. Choudhury, *Status of the MSSM Higgs sector using global analysis and direct search bounds, and future prospects at the High Luminosity LHC*, Phys. Rev. **D92** no. 9, (2015) 093007, arXiv:1504.04308 [hep-ph].
- [27] CMS Collaboration, S. Chatrchyan et al., *Searches for new physics using the $t\bar{t}$ invariant mass distribution in pp collisions at $\sqrt{s}=8\text{TeV}$* , Phys. Rev. Lett. **111** no. 21, (2013) 211804, arXiv:1309.2030 [hep-ex]. [Erratum: Phys. Rev. Lett.112,119903(2014)].
- [28] ATLAS Collaboration, G. Aad et al., *A search for $t\bar{t}$ resonances using lepton-plus-jets events in proton-proton collisions at $\sqrt{s} = 8 \text{ TeV}$ with the ATLAS detector*, JHEP **08** (2015) 148, arXiv:1505.07018 [hep-ex].
- [29] M. Kramer, E. Laenen, and M. Spira, *Soft gluon radiation in Higgs boson production at the LHC*, Nucl. Phys. **B511** (1998) 523–549, arXiv:hep-ph/9611272 [hep-ph].
- [30] J. C. Collins and D. E. Soper, *Angular Distribution of Dileptons in High-Energy Hadron Collisions*, Phys. Rev. **D16** (1977) 2219.
- [31] A. W. El Kaffas, W. Khater, O. M. Ogreid, and P. Osland, *Consistency of the two Higgs doublet model and CP violation in top production at the LHC*, Nucl. Phys. **B775** (2007) 45–77, arXiv:hep-ph/0605142 [hep-ph].
- [32] B. Grzadkowski, O. M. Ogreid, and P. Osland, *Measuring CP violation in Two-Higgs-Doublet models in light of the LHC Higgs data*, JHEP **11** (2014) 084, arXiv:1409.7265 [hep-ph].
- [33] W. Bernreuther, T. Schroder, and T. N. Pham, *CP violating dipole form-factors in $e^+e^- \rightarrow t\bar{t}$* , Phys. Lett. **B279** (1992) 389–396.
- [34] S. Inoue, M. J. Ramsey-Musolf, and Y. Zhang, *CP-violating phenomenology of flavor conserving two Higgs doublet models*, Phys. Rev. **D89** no. 11, (2014) 115023, arXiv:1403.4257 [hep-ph].
- [35] C.-Y. Chen, S. Dawson, and Y. Zhang, *Complementarity of LHC and EDMs for Exploring Higgs CP Violation*, JHEP **06** (2015) 056, arXiv:1503.01114 [hep-ph].

- [36] C. Mellein, *Doctoral Thesis, RWTH Aachen University (2015), unpublished.*
- [37] F. Mahmoudi and O. Stal, *Flavor constraints on the two-Higgs-doublet model with general Yukawa couplings*, Phys. Rev. **D81** (2010) 035016, arXiv:0907.1791 [hep-ph].
- [38] T. Hermann, M. Misiak, and M. Steinhauser, $\bar{B} \rightarrow X_s \gamma$ in the Two Higgs Doublet Model up to Next-to-Next-to-Leading Order in QCD, JHEP **11** (2012) 036, arXiv:1208.2788 [hep-ph].
- [39] O. Eberhardt, U. Nierste, and M. Wiebusch, *Status of the two-Higgs-doublet model of type II*, JHEP **07** (2013) 118, arXiv:1305.1649 [hep-ph].
- [40] A. Djouadi, J. Kalinowski, and M. Spira, *HDECAY: A Program for Higgs boson decays in the standard model and its supersymmetric extension*, Comput. Phys. Commun. **108** (1998) 56–74, arXiv:hep-ph/9704448 [hep-ph].
- [41] D. Eriksson, J. Rathsman, and O. Stal, *2HDMC: Two-Higgs-Doublet Model Calculator Physics and Manual*, Comput. Phys. Commun. **181** (2010) 189–205, arXiv:0902.0851 [hep-ph].
- [42] E. Braaten and J. P. Leveille, *Higgs Boson Decay and the Running Mass*, Phys. Rev. **D22** (1980) 715.
- [43] M. Drees and K.-i. Hikasa, *NOTE ON QCD CORRECTIONS TO HADRONIC HIGGS DECAY*, Phys. Lett. **B240** (1990) 455. [Erratum: Phys. Lett.B262,497(1991)].
- [44] M. Spira, A. Djouadi, D. Graudenz, and P. M. Zerwas, *Higgs boson production at the LHC*, Nucl. Phys. **B453** (1995) 17–82, arXiv:hep-ph/9504378 [hep-ph].
- [45] A. Dabelstein and W. Hollik, *Electroweak corrections to the fermionic decay width of the standard Higgs boson*, Z. Phys. **C53** (1992) 507–516.
- [46] J. Fleischer and F. Jegerlehner, *Radiative Corrections to Higgs Decays in the Extended Weinberg-Salam Model*, Phys. Rev. **D23** (1981) 2001–2026.
- [47] W. Grimus, L. Lavoura, O. M. Ogreid, and P. Osland, *A Precision constraint on multi-Higgs-doublet models*, J. Phys. **G35** (2008) 075001, arXiv:0711.4022 [hep-ph].
- [48] W. Grimus, L. Lavoura, O. M. Ogreid, and P. Osland, *The Oblique parameters in multi-Higgs-doublet models*, Nucl. Phys. **B801** (2008) 81–96, arXiv:0802.4353 [hep-ph].
- [49] H. E. Haber and D. O’Neil, *Basis-independent methods for the two-Higgs-doublet model III: The CP-conserving limit, custodial symmetry, and the oblique parameters S, T, U*, Phys. Rev. **D83** (2011) 055017, arXiv:1011.6188 [hep-ph].
- [50] C. A. Baker et al., *An Improved experimental limit on the electric dipole moment of the neutron*, Phys. Rev. Lett. **97** (2006) 131801, arXiv:hep-ex/0602020 [hep-ex].

- [51] ACME Collaboration, J. Baron et al., *Order of Magnitude Smaller Limit on the Electric Dipole Moment of the Electron*, *Science* **343** (2014) 269–272, arXiv:1310.7534 [physics.atom-ph].
- [52] J. H. Kuhn, A. Scharf, and P. Uwer, *Weak Interactions in Top-Quark Pair Production at Hadron Colliders: An Update*, *Phys. Rev.* **D91** no. 1, (2015) 014020, arXiv:1305.5773 [hep-ph].
- [53] P. Nason, S. Dawson, and R. K. Ellis, *The Total Cross-Section for the Production of Heavy Quarks in Hadronic Collisions*, *Nucl. Phys.* **B303** (1988) 607.
- [54] W. Beenakker, H. Kuijf, W. L. van Neerven, and J. Smith, *QCD Corrections to Heavy Quark Production in p anti- p Collisions*, *Phys. Rev.* **D40** (1989) 54–82.
- [55] A. Denner, S. Dittmaier, M. Roth, and D. Wackerroth, *Predictions for all processes $e^+e^- \rightarrow 4$ fermions + γ* , *Nucl. Phys.* **B560** (1999) 33–65, arXiv:hep-ph/9904472 [hep-ph].
- [56] A. Denner, S. Dittmaier, M. Roth, and L. H. Wieders, *Electroweak corrections to charged-current $e^+e^- \rightarrow 4$ fermion processes: Technical details and further results*, *Nucl. Phys.* **B724** (2005) 247–294, arXiv:hep-ph/0505042 [hep-ph]. [Erratum: *Nucl. Phys.*B854,504(2012)].
- [57] M. Nowakowski and A. Pilaftsis, *On gauge invariance of Breit-Wigner propagators*, *Z. Phys.* **C60** (1993) 121–126, arXiv:hep-ph/9305321 [hep-ph].
- [58] R. Harlander and P. Kant, *Higgs production and decay: Analytic results at next-to-leading order QCD*, *JHEP* **12** (2005) 015, arXiv:hep-ph/0509189 [hep-ph].
- [59] A. Djouadi, M. Spira, and P. M. Zerwas, *Production of Higgs bosons in proton colliders: QCD corrections*, *Phys. Lett.* **B264** (1991) 440–446.
- [60] R. V. Harlander and W. B. Kilgore, *Soft and virtual corrections to proton proton to $H + x$ at NNLO*, *Phys. Rev.* **D64** (2001) 013015, arXiv:hep-ph/0102241 [hep-ph].
- [61] K. G. Chetyrkin, B. A. Kniehl, M. Steinhauser, and W. A. Bardeen, *Effective QCD interactions of CP odd Higgs bosons at three loops*, *Nucl. Phys.* **B535** (1998) 3–18, arXiv:hep-ph/9807241 [hep-ph].
- [62] R. V. Harlander and W. B. Kilgore, *Production of a pseudoscalar Higgs boson at hadron colliders at next-to-next-to leading order*, *JHEP* **10** (2002) 017, arXiv:hep-ph/0208096 [hep-ph].
- [63] V. S. Fadin, V. A. Khoze, and A. D. Martin, *Interference radiative phenomena in the production of heavy unstable particles*, *Phys. Rev.* **D49** (1994) 2247–2256.
- [64] K. Melnikov and O. I. Yakovlev, *Final state interaction in the production of heavy unstable particles*, *Nucl. Phys.* **B471** (1996) 90–120, arXiv:hep-ph/9501358

[hep-ph].

- [65] W. Beenakker, A. P. Chapovsky, and F. A. Berends, *Nonfactorizable corrections to W pair production: Methods and analytic results*, Nucl. Phys. **B508** (1997) 17–63, arXiv:hep-ph/9707326 [hep-ph].
- [66] S. Dittmaier, A. Huss, and C. Schwinn, *Mixed QCD-electroweak $O(\alpha_s\alpha)$ corrections to Drell-Yan processes in the resonance region: pole approximation and non-factorizable corrections*, Nucl. Phys. **B885** (2014) 318–372, arXiv:1403.3216 [hep-ph].
- [67] P. Nason, S. Dawson, and R. K. Ellis, *The One Particle Inclusive Differential Cross-Section for Heavy Quark Production in Hadronic Collisions*, Nucl. Phys. **B327** (1989) 49–92. [Erratum: Nucl. Phys.B335,260(1990)].
- [68] W. Beenakker, W. L. van Neerven, R. Meng, G. A. Schuler, and J. Smith, *QCD corrections to heavy quark production in hadron hadron collisions*, Nucl. Phys. **B351** (1991) 507–560.
- [69] W. Bernreuther, A. Brandenburg, Z. G. Si, and P. Uwer, *Top quark spin correlations at hadron colliders: Predictions at next-to-leading order QCD*, Phys. Rev. Lett. **87** (2001) 242002, arXiv:hep-ph/0107086 [hep-ph].
- [70] W. Bernreuther, A. Brandenburg, Z. G. Si, and P. Uwer, *Top quark pair production and decay at hadron colliders*, Nucl. Phys. **B690** (2004) 81–137, arXiv:hep-ph/0403035 [hep-ph].
- [71] G. Passarino and M. J. G. Veltman, *One Loop Corrections for e^+e^- Annihilation Into $\mu^+\mu^-$ in the Weinberg Model*, Nucl. Phys. **B160** (1979) 151.
- [72] W. Bernreuther, R. Bonciani, T. Gehrmann, R. Heinesch, P. Mastrolia, and E. Remiddi, *Decays of scalar and pseudoscalar Higgs bosons into fermions: Two-loop QCD corrections to the Higgs-quark-antiquark amplitude*, Phys. Rev. **D72** (2005) 096002, arXiv:hep-ph/0508254 [hep-ph].
- [73] S. Catani and M. H. Seymour, *A General algorithm for calculating jet cross-sections in NLO QCD*, Nucl. Phys. **B485** (1997) 291–419, arXiv:hep-ph/9605323 [hep-ph]. [Erratum: Nucl. Phys.B510,503(1998)].
- [74] S. Catani, S. Dittmaier, M. H. Seymour, and Z. Trocsanyi, *The Dipole formalism for next-to-leading order QCD calculations with massive partons*, Nucl. Phys. **B627** (2002) 189–265, arXiv:hep-ph/0201036 [hep-ph].
- [75] W. Bernreuther and Z.-G. Si, *Distributions and correlations for top quark pair production and decay at the Tevatron and LHC.*, Nucl. Phys. **B837** (2010) 90–121, arXiv:1003.3926 [hep-ph].
- [76] H.-L. Lai, M. Guzzi, J. Huston, Z. Li, P. M. Nadolsky, J. Pumplin, and C. P. Yuan, *New parton distributions for collider physics*, Phys. Rev. **D82** (2010) 074024, arXiv:1007.2241 [hep-ph].

- [77] LHC Higgs Cross Section Working Group Collaboration, S. Dittmaier et al., *Handbook of LHC Higgs Cross Sections: 1. Inclusive Observables*, arXiv:1101.0593 [hep-ph].
- [78] CMS Collaboration, S. Chatrchyan et al., *Measurement of the $t\bar{t}$ production cross section in the dilepton channel in pp collisions at $\sqrt{s} = 8$ TeV*, JHEP **02** (2014) 024, arXiv:1312.7582 [hep-ex]. [Erratum: JHEP02,102(2014)].
- [79] CMS Collaboration, V. Khachatryan et al., *Measurement of the differential cross section for top quark pair production in pp collisions at $\sqrt{s} = 8$ TeV*, Eur. Phys. J. **C75** no. 11, (2015) 542, arXiv:1505.04480 [hep-ex].
- [80] T. P. Li and Y. Q. Ma, *Analysis methods for results in gamma-ray astronomy*, Astrophys. J. **272** (1983) 317–324.
- [81] R. D. Cousins, J. T. Linnemann, and J. Tucker, *Evaluation of three methods for calculating statistical significance when incorporating a systematic uncertainty into a test of the background-only hypothesis for a Poisson process*, Nucl. Instrum. Meth. **A595** (2008) 480–501.
- [82] M. Czakon, P. Fiedler, and A. Mitov, *Total Top-Quark Pair-Production Cross Section at Hadron Colliders Through $O(\alpha_s^4)$* , Phys. Rev. Lett. **110** (2013) 252004, arXiv:1303.6254 [hep-ph].
- [83] M. Czakon, D. Heymes, and A. Mitov, *High-precision differential predictions for top-quark pairs at the LHC*, arXiv:1511.00549 [hep-ph].
- [84] P. Uwer, *EasyNData: A Simple tool to extract numerical values from published plots*, arXiv:0710.2896 [physics.comp-ph].